Title

Systematic engineering for production of anti-aging sunscreen compound in Pseudomonas putida

Authors

Yunus, Ian S

Hudson, Graham A

Chen, Yan

et al.

Publication Date

2024-07-01

DOI

10.1016/j.ymben.2024.06.001

Systematic engineering for production of anti-aging sunscreen compound in *Pseudomonas putida*

Ian S. Yunus[1,2,*], Graham A. Hudson[1,2,3], Yan Chen[1,2], Jennifer W. Gin[1,2], Joonhoon Kim[1,4], Edward E. K. Baidoo[1,2], Christopher J. Petzold[1,2], Paul D. Adams[1,5], Blake A. Simmons[1,2], Aindrila Mukhopadhyay[1,2], Jay D. Keasling[1,2,3,6,7,8], and Taek Soon Lee[1,2,*]

[1]Joint BioEnergy Institute, 5885 Hollis Street, Emeryville, CA, USA
[2]Biological Systems & Engineering Division, Lawrence Berkeley National Laboratory, Berkeley, CA, USA
[3]California Institute of Quantitative Biosciences (QB3), University of California, Berkeley, CA, USA
[4]Energy Processes & Materials Division, Pacific Northwest National Laboratory, Richland, WA, USA
[5]Molecular Biophysics & Integrated Bioimaging Division, Lawrence Berkeley National Laboratory, Berkeley, CA, USA
[6]Department of Chemical & Biomolecular Engineering, University of California, Berkeley, CA, USA.
[7]Department of Bioengineering, University of California, Berkeley, CA, USA.
[8]Center for Biosustainability, Danish Technical University, Lyngby, Denmark

*Corresponding Authors, Joint BioEnergy Institute, 5885 Hollis Street, Emeryville, CA 94608, USA.
E-mail addresses: tslee@lbl.gov (T. S. Lee). Tel: +1-510-495-2470. Fax: +1-510-495-2629; iansofianyunus@gmail.com (I. S. Yunus).

Abstract

Sunscreen has been used for thousands of years to protect skin from ultraviolet radiation. However, the use of modern commercial sunscreen containing oxybenzone, ZnO, and TiO_2 has raised concerns due to their negative effects on human health and the environment. In this study, we aim to establish an efficient microbial platform for production of shinorine, a UV light absorbing compound with anti-aging properties. First, we methodically selected an appropriate host for shinorine production by analyzing central carbon flux distribution data from prior studies alongside predictions from genome-scale metabolic models (GEMs). We enhanced shinorine productivity

through CRISPRi-mediated downregulation and utilized shotgun proteomics to pinpoint potential competing pathways. Simultaneously, we improved the shinorine biosynthetic pathway by refining its design, optimizing promoter usage, and altering the strength of ribosome binding sites. Finally, we conducted amino acid feeding experiments under various conditions to identify the key limiting factors in shinorine production. The study combines meta-analysis of ^{13}C-metabolic flux analysis, GEMs, synthetic biology, CRISPRi-mediated gene downregulation, and omics analysis to improve shinorine production, demonstrating the potential of *Pseudomonas putida* KT2440 as platform for shinorine production.

Keywords: *natural products, mycosporine-like amino acid (MAA), CRISPR interference (CRISPRi), Pseudomonas, genome-scale model, proteomics*

Highlights:

- Meta-analysis of ^{13}C-MFA and GEMs show *P. putida* to be an ideal host for shinorine production.
- CRISPRi-mediated gene downregulation of PP_1444 improves shinorine production.
- Shinorine was produced at high titers and amino acid supplementation improved the titer.
- Shinorine accumulates exclusively in the supernatant in *P. putida* cultures.

1. Introduction

Extended warm periods (Oliver et al., 2018), global warming (Johnson et al., 2022), and excessive use of chemical sunscreens (Roberto et al., 2008) have been linked to world-wide coral bleaching. Due to concerns about their adverse effects on both human health and the environment, several countries and regions have prohibited the use of commercial sunscreens containing oxybenzone, octinoxate, ZnO, and TiO_2. This has led to a rising demand for sunscreens derived from environmentally friendly sources. Shinorine, a mycosporine-like amino acid (MAA) typically produced by red algae *Porphyra umbilicalis*, has been used as an active ingredient in commercial sunscreen products (e.g., Helioguard™ 365, Helionori®). Shinorine has also demonstrated additional benefits including anti-aging properties, antioxidant effects, promotion of wound healing, and inhibition of UV radiation-induced skin inflammation (Choi et al., 2015; Hartmann et al., 2015; Orfanoudaki et al., 2020; Suh et al., 2014; Torres et al., 2018). The yield of shinorine from *P. umbilicalis*, however, is low (3.27 mg/g cell dry weight) (Becker et al., 2016), and its production suffers from the slow growth of *P. umbilicalis*. With the continuous rise in global demand for sunscreen, the bioproduction of shinorine in a fast-growing microbe emerges as an attractive solution.

To meet the growing demand of shinorine, various host organisms, including *Saccharomyces cerevisiae* (Jin et al., 2021; Kim et al., 2023, 2022; Park et al., 2019), *Corynebacterium glutamicum* (Tsuge et al., 2018), *Synechocystis* sp. PCC 6803 (Yang et al., 2018), *Streptomyces avermitilis* (Miyamoto et al., 2014), and *Yarrowia lipolytica* (Jin et al., 2023), have been genetically engineered for shinorine production. Most metabolic engineering efforts within the aforementioned host organisms, however, have primarily focused on coupling the shinorine production pathway with the xylose utilization pathway to enhance the xylulose 5-phosphate pool (Jin et al., 2023; Kim et al., 2023, 2022; Park et al., 2019). While this approach has been proven to improve the shinorine titers, challenges persist. The highest shinorine productivity (12.75 mg/L/h) and yield (36 mg/g total sugar) were achieved in *Saccharomyces cerevisiae* in a fed-batch bioreactor (Kim et al., 2023). However, supplying sugar mixtures (e.g., hexoses and pentoses) into cultures introduces complexities to production experiments (Park et al., 2019), as microbial hosts typically exhibit a preference for hexose (e.g., glucose) consumption over pentose (e.g., xylose) (Aidelberg et al., 2014; Dvořák and de Lorenzo, 2018; Yan Wang et al., 2019). Additionally, a large portion of shinorine produced from *S. cerevisiae* and *Y. lipolytica* tends to accumulate within the cells (Jin et al., 2023; Kim et al., 2023), complicating extraction and purification.

In this study, we methodically selected an appropriate host for shinorine production by analyzing central carbon flux distribution data from prior studies alongside predictions from genome-scale metabolic models (GEMs). We identified *Pseudomonas putida* KT2440 as a promising host for shinorine production. We then developed synthetic biology tools for use in this microbe and heterologously expressed shinorine biosynthetic gene cluster (BGC) from *Anabaena variabilis* ATCC 29413. We enhanced shinorine productivity through CRISPRi-mediated downregulation of potential competing pathways. Simultaneously, we improved the shinorine biosynthetic pathway by refining its design, optimizing promoter usage, and altering the strength of ribosome binding sites. Finally, we conducted amino acid feeding experiments under various conditions and utilized shotgun proteomics to identify the limiting factors in shinorine production. Altogether, our study provides a comprehensive framework for engineering *P. putida* KT2440 as an efficient chassis for shinorine production.

2. Results and Discussion

2.1 Selection of *P. putida* KT2440 as a suitable host for shinorine production

To select a suitable host for shinorine production, we reviewed published metabolic flux distribution from commonly used biomanufacturing hosts with available ^{13}C-metabolic flux analysis (MFA) data (Figure 1, Supplementary Table S1) alongside predictions from genome-scale metabolic models (GEMs) (Supplementary Table S2). We primarily focused on analyzing fluxes directed towards 6-phosphogluconate (6PG) as this intermediary metabolite plays important roles in the shinorine biosynthetic pathway. 6PG functions as an intermediate molecule in both the pentose-phosphate and the Entner-Doudoroff pathways. In the pentose-phosphate pathway, 6PG undergoes decarboxylation to produce ribulose 5-phosphate (Ru5P), which is further metabolized into ribose 5-phosphate (R5P) and xylulose 5-phosphate (X5P) by ribulose-5-phosphate epimerase. While R5P serves as a fundamental building block for nucleic acid synthesis, X5P is converted by a transketolase to glyceraldehyde 3-phosphate (G3P) and sedoheptulose 7-phosphate (S7P), acting as a precursor for shinorine biosynthesis. G3P is converted to 3-phopshoglycerate (3PG) through either glycolysis (the Embden-Meyerhof-Parnas (EMP) pathway) or the Entner-Doudoroff pathway. 3PG is used for the biosynthesis of *L*-serine and glycine, essential amino acids incorporated into the shinorine biosynthetic pathway.

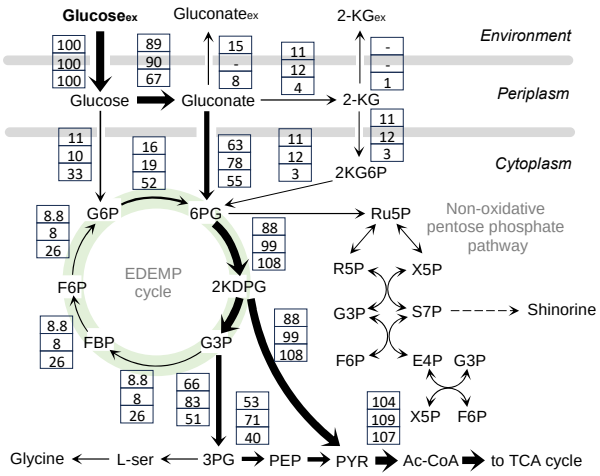

Figure 1. Metabolic flux distribution of glucose-fed *Pseudomonas putida* KT2440. All values in boxes are given as relative fluxes normalized to the specific glucose uptake rate. Data are referenced from three primary studies: (Kukurugya et al., 2019) (top), (Nikel et al., 2015) (middle), and (Kohlstedt and Wittmann, 2019) (bottom). Arrow widths are proportional to the average of the three values. Abbreviations: G6P, glucose 6-phosphate; F6P, fructose 6-phosphate; FBP, fructose-1,6-biphosphate; DHAP, dihydroxyacetone phosphate; 6PG, 6-phosphogluconate; KDPG, 2-keto-3-deoxy-6-phosphogluconate; Ru5P, ribulose 5-phosphate; R5P, ribose 5-phosphate; X5P, xylulose 5-phosphate; S7P, sedoheptulose 7-phosphate; E4P, erythrose 4-phosphate; G3P, glyceraldehyde 3-phosphate; 3PG, 3-phosphoglycerate; PEP, phosphoenolpyruvate; Ac-CoA, acetyl-coenzyme A; L-ser, L-serine; TCA, tricarboxylic acid; PYR, pyruvate

In most organisms, except for *P. putida* KT2440 and *Bacillus megatarium* QM B1551, glucose is directly phosphorylated by glucokinase, producing glucose 6-phosphate (G6P) (Fig. 1, Supplementary Figure S1). G6P can be either isomerized to fructose 6-phosphate (F6P) within the glycolytic pathway or undergo oxidation to form 6PG through the oxidative pentose phosphate pathway. The carbon flux distribution from G6P to F6P or G6P to 6PG, as determined through ^{13}C metabolic flux analysis (^{13}C-MFA), varies among different microorganisms and is influenced by factors such as fermentation conditions and genetic variations (Supplementary Table S1). Nonetheless, meta-analysis of ^{13}C-MFA and predictions from GEMs (Supplementary Table S2) reveal that only a few microbes can allocate more than 50% of their carbon flux towards 6PG.

Zymomonas mobilis converts approximately 99% of its glucose supply to 6PG (Supplementary Table S1). However, the oxidative branch of the pentose phosphate pathway in *Z. mobilis* appears inactive as *Z. mobilis* lacks 6PG dehydrogenase enzyme (De Graaf et al., 1999; Jacobson et al., 2019). Instead of using the oxidative branch of the pentose phosphate pathway, *Z. mobilis* uses the non-oxidative branch and converts F6P to R5P and S7P through a series of enzymatic reactions. Only 0.8% carbon flux is distributed from G6P to F6P, leaving a very small pool of F6P for S7P synthesis. On the other hand, *in silico* metabolic network analysis

of *Rhodosporidium toruloides* reveals that glucose-fed *R. toruloides* allocates 89.7% of its carbon flux towards 6PG, creating a significant pool of S7P in the non-oxidative pentose phosphate pathway (Bommareddy et al., 2015). *R. toruloides* is also an attractive host for industrial scale production of many chemical compounds (Liu et al., 2023, 2020; Schultz et al., 2022; Wehrs et al., 2019). It can readily co-consume C5 and C6 sugars derived from lignocellulosic biomass and grows to very high cell density. However, engineering *R. toruloides* has been challenging (Wen et al., 2020) with only a few synthetic biology tools available (Brink et al., 2023).

P. putida KT2440 exhibits a distinctive central carbon metabolism (Fig. 1). In this microbe, glucose can be phosphorylated to G6P in the cytoplasm through direct phosphorylation, or it can undergo oxidation to gluconate catalyzed by glucose dehydrogenase in the periplasm. Subsequently, gluconate can follow one of two routes: it can be phosphorylated to 6PG by gluconokinase in the cytoplasm or oxidized to 2-ketogluconate (2-KG) in the periplasm. The latter compound, 2-KG, is then transported into the cytoplasm and converted to 2-keto-6-phosphogluconate (2K6PG) by 2-KG kinase, which is further reduced to 6PG by 2K6PG reductase. While most glucose is oxidized to gluconate, regardless of the initial step in glucose processing, these pathways converge into the production of 6PG. Furthermore, in contrast to other microorganisms, *P. putida* KT2440 favors the conversion of F6P to 6PG rather than the reverse reaction. As a result, *P. putida* KT2440 converts over 90% of its glucose supply to 6PG, creating a substantial pool of 6PG for the biosynthesis of Ru5P and S7P in the non-oxidative pentose-phosphate pathway. In addition, genome editing and synthetic biology tools for *P. putida* KT2440 have been widely available and well characterized (Nikel and de Lorenzo, 2018). This unique metabolic trait positions *P. putida* KT2440 as a promising host for shinorine production.

2.2 Development of synthetic biology tools for gene expression in *P. putida* KT2440

To establish the shinorine biosynthetic pathway, we began by first developing a modular plasmid assembly tool for use in *P. putida* KT2440 (Fig. 2A). Here, we used Biopart Assembly Standard for Idempotent Cloning (BASIC) (Storch et al., 2015) plasmid assembly method to allow multipart DNA assembly using standard reusable parts in a single pot assembly reaction. The resulting expression plasmids were then used to assess the functionality of genetic elements, such as promoters and ribosome binding sites. The primary objective of this effort was not an exhaustive characterization of the genetic elements but rather an investigation of the performance of the expression plasmid and individual genetic elements employed in this study.

Six plasmids (pBBR1, pBBR1-B5, pRK2, pRSF1010, pRO1600/p15a, and pVS1/p15a) with distinct backbones, copy numbers, and origin of replications were constructed and characterized (Fig. 2B) by measuring the fluorescence intensity of a red fluorescent protein (RFP). The plasmids selected for construction offer diverse features. First, pBBR1, isolated from *Bordetella bronchiseptica* S87 (Antoine and Locht, 1992), is a broad host range plasmid origin commonly used for gene expression in metabolic engineering studies of *P. putida* (Niu et al., 2020; Tiso et al., 2016; X. Wang et al., 2022; Wohlers et al., 2021). Although generally considered a low- to medium-copy plasmid with 30 copies per chromosome (Cook et al., 2018), the copy number of pBBR1 can be altered by mutations in the *rep* gene (Tao et al., 2005). Second, pBBR1-B5, a variant of pBBR1 plasmid with an early stop codon in the *rep* gene, exhibits around 70 copies per chromosome, a higher copy number than the original pBBR1 plasmid. Third, the plasmid pRK2 is a member of the IncP incompatibility group and requires an origin of replication and a replication initiation protein encoded by *trfA* to function. It has been shown to be stably maintained in *P. putida* and has been measured to be a low-copy plasmid in *Escherichia coli* ((De Bernardez and Dhurjati, 1987) and has around 30 copies per chromosome in *P. putida* (Cook et al., 2018). Fourth, RSF1010 is a high-copy broad host range plasmid with 130 copies per chromosome and is a part of the IncQ incompatibility group plasmid. It has been routinely used for gene expression in *P. putida* (Aparicio et al., 2019). Lastly, pRO1600 (Farinha and Kropinski, 1990) and pVS1 (Itoh and Haas, 1985) are plasmids isolated from *Pseudomonas* species, requiring host-specific origins (e.g., p15a, that replicates in *E. coli*) to generate shuttle vectors for *P. putida*. In this study, plasmid characterization reveals that pBBR1-B5 shows the highest RFP fluorescence level, followed by pBBR1 > pRSF1010 = pRO1600/p15a > pRK2 > pVS1/p15a plasmids (Figure 2C).

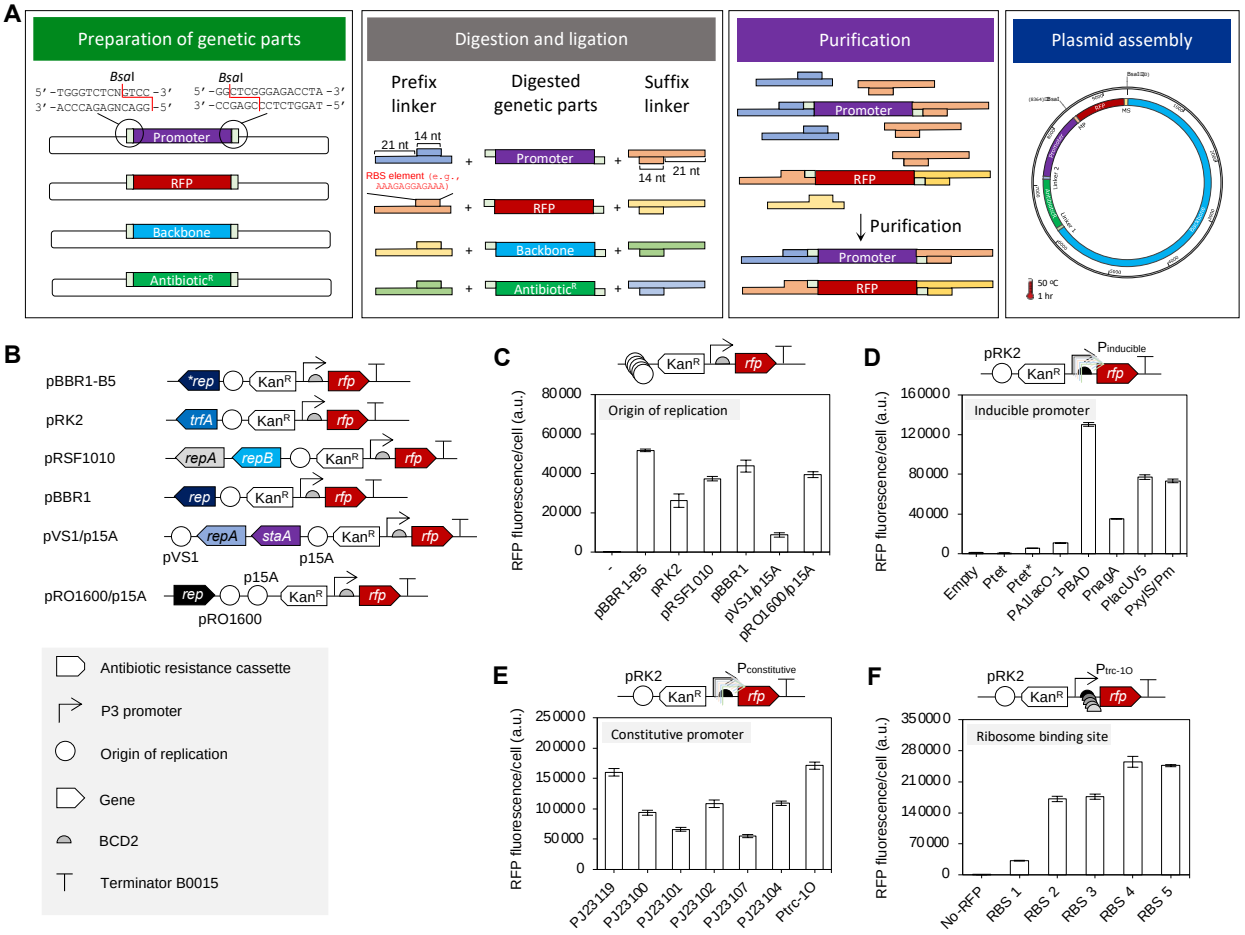

Figure 2. Development of genetic tools for gene expression in *Pseudomonas putida* KT2440. (A) Modular cloning assembly method as described in a previously published work (Storch et al., 2015). Genetic parts were cloned into a pJET1.2 blunt DNA plasmid. Subsequently, these parts were digested with *BsaI* restriction enzyme and ligated with prefix and suffix linkers, followed by separation and purification using magnetic beads. Finally, purified genetic parts and linkers were assembled in one-pot reaction at 50 °C for 1 h. (B) Schematic diagrams of plasmids with different backbones. RFP fluorescence levels measured across various plasmid backbones (C), under different inducible promoters (D), constitutive promoters (E), and ribosome binding site sequences (F). Cultures were grown in 5 mL of M9 minimal medium. RFP fluorescence was measured using a flow cytometer at 48 hr post-inoculation. Inducer was added at 0 h. Error bars represent the standard deviation of three biological replicates.

Given its medium-range RFP fluorescence, plasmid pRK2 was then selected as the plasmid backbone for the characterization of different inducible (Figure 2D) and constitutive (Figure 2E) promoters. Seven different inducible promoters (P_{tet} (Cook et al., 2018), P_{tet*} (Tian et al., 2019), $P_{A1lacO-1}$ (Liu et al., 2019), P_{BAD} (Calero et al., 2016), P_{NagA} (Hüsken et al., 2001), P_{lacUV5} (Noel Jr. and Reznikoff, 2000), and $P_{XylS/Pm}$ (Calero et al., 2016)), six constitutive promoters (Anderson et al., 2010) with varying strength (P_{J23119}, P_{J23100}, P_{J23101}, P_{J23102}, P_{J23107}, P_{J23104}), and P_{trc1-O} (Bagdasarian et al., 1983; Calero et al., 2016) (without a LacI repressor) were characterized.

P_{tet} and $P_{A1lacO-1}$ promoters exhibited a high basal fluorescence level (Supplementary Figure S2) compared to other promoters. Among the inducible promoters, P_{BAD}, the arabinose-inducible promoter, showed the highest RFP fluorescence level. Meanwhile, under the conditions tested, the constitutive promoter P_{trc-1O} was the strongest promoter among all evaluated promoters.

Lastly, we characterized ribosome binding site (RBS) elements tailored for application in *P. putida* KT2440. The use of RBSs with varying strengths has been employed in metabolic engineering studies, proving to be a useful strategy for pathway optimization. Despite its significance, RBS characterization in *P. putida* has only been described in a few studies. First, Elmore and colleagues characterized ten different RBS elements by mutating four nucleotides within the core RBS sequence (Elmore et al., 2017). In combination with different promoters, the RBS they generated exhibited up to 7-fold differences in the expression levels of mNeonGreen. In another study, Damalas and colleagues leveraged the RBS calculator (Salis, 2011) to computationally predic six RBS sequences. These RBS sequences, compatible with The Standard European Vector Architecture (SEVA) platform or the BioBrick assembly, expanded the synthetic biology toolkit in *P. putida* (Damalas et al., 2020). In the following study, Aparicio and colleagues employed recombineering techniques to generate a library of 33 RBS variants (Aparicio et al., 2020). Unique to those studies, here, we embedded an RBS element into a prefix linker (Fig. 2A) to enable the flexible placement of RBS linker upstream of the coding sequence of any gene of interest. We selected three RBS sequences from BioBrick (Shetty et al., 2008) (RBS1; ATCACACAGGAC (BBa_B0033), RBS2; AAAGAGGGGAAA (Bba_B0064), and RBS3; AAAGAGGAGAAA (Bba_B0034)), a Shine-Dalgarno *E. coli* consensus (RBS4; ATCACAAGGAGG), and an anti-Shine-Dalgarno complementary sequence (RBS5: ATTAGTGGAGGT). These RBS linkers have previously been characterized in *E. coli* (Storch et al., 2015), demonstrating a wide range of fluorescent protein expression levels. However, these RBS linkers are yet to be characterized in *P. putida*.

Evaluation of the RBS linkers in *P. putida* revealed that the selected ribosome binding sites exhibited varying strengths, low (RBS 1), medium (RBS 2 and RBS 3), and high (RBS 4 and 5) with an 8-fold difference between the weakest and strongest RBS (Fig. 2F). We anticipate that when combined with different promoters, these selected RBS elements will provide a diverse array of options for fine-tuning and optimizing biosynthetic pathways in future studies. All in all, the characterization of these genetic elements, alongside the introduction of linker-based modular cloning assembly method tailored for *P. putida* KT2440, heralds an expansion of the synthetic biology toolkit for this organism. Such progress paves the path for more efficient and customized metabolic engineering efforts in *P. putida*.

2.3 Shinorine production in *Pseudomonas putida* KT2440

After evaluating the performance and functionality of plasmid backbones, promoters, and ribosome binding sites in *P. putida* KT2440, we began constructing the shinorine biosynthetic pathway (Fig. 3A). The shinorine biosynthetic gene cluster (BGC) has been identified in various microorganisms, including *Anabaena variabilis* ATCC 29413 (Emily P Balskus and Walsh, 2010), *Nostoc punctiforme* ATCC 29133/PCC 73102 (Qunjie and Ferran, 2011), *Actinosynnema mirum* DSM 43827 (Miyamoto et al., 2014), *Chlorogloeopsis fritschii* PCC 6912 (Llewellyn et al., 2020; Portwich and Garcia-Pichel, 2003), and *Fischerella* sp. PCC 9339 (Yang et al., 2018). In this study, we selected the shinorine biosynthetic pathway from *Anabaena variabilis* ATCC 29413 and *Nostoc punctiforme* ATCC 29133 as the two BGCs have been used for shinorine biosynthesis in various organisms (Jin et al., 2023; Kim et al., 2023; Park et al., 2019). S7P, an intermediate metabolite of the pentose phosphate pathway, is converted into shinorine through a series of four enzymatic steps. Firstly, S7P undergoes transformation into 4-deoxygadusol (4-DG) by 2-demethyl 4-deoxygadusol synthase (DDGS) and *O*-methyltransferase (O-MT). Subsequently, glycine is conjugated to 4-DG by ATP-grasp ligase to form mycosporine-glycine (MG). Finally, a serine moiety is attached to MG by a nonribosomal peptide synthetase (NRPS)-like enzyme in *Anabaena variabilis* ATCC 29413 or by a D-Ala-D-Ala ligase in *Nostoc punctiforme* ATCC 29133 (Fig. 3A,B).

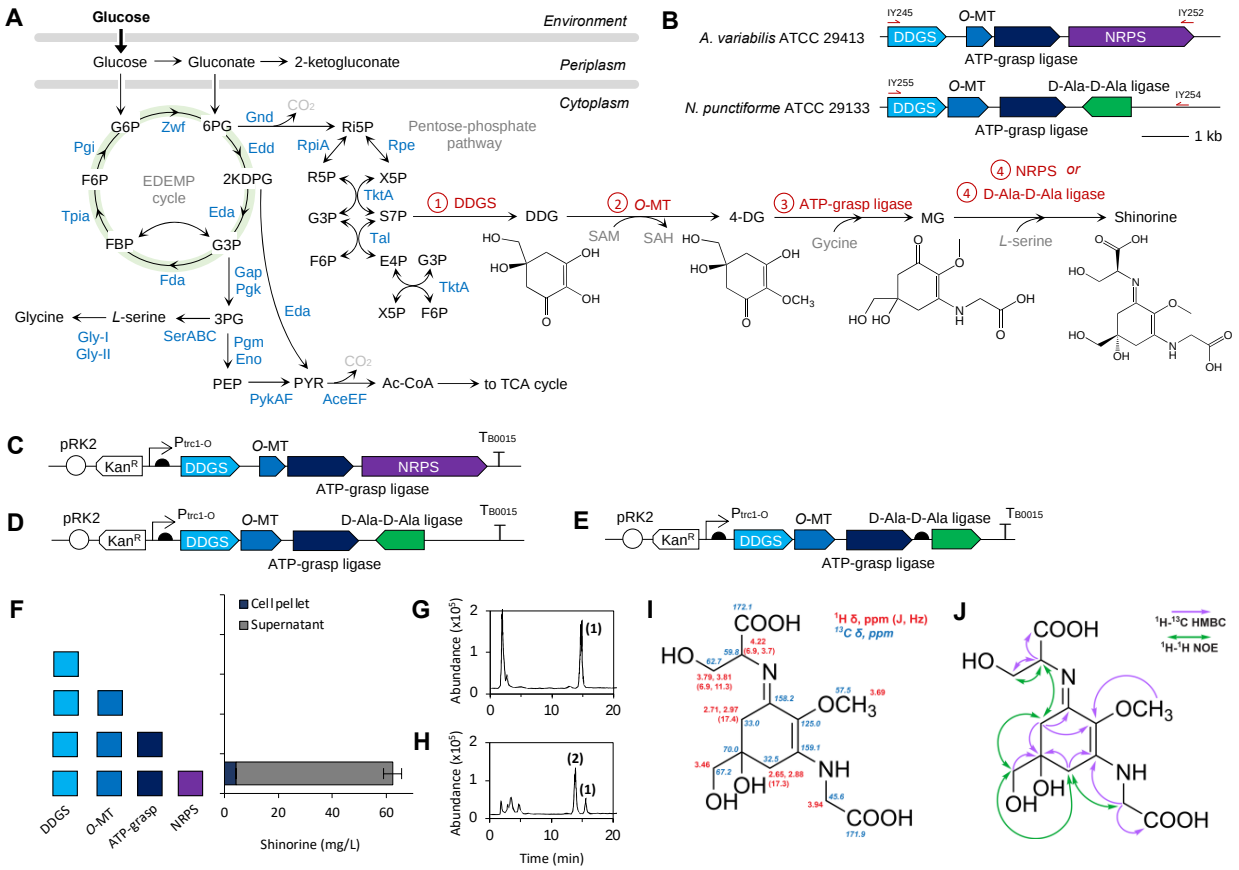

Figure 3. Production experiment of shinorine in engineered *P. putida* KT2440 and confirmation by nuclear magnetic resonance (NMR) spectroscopy. (A) Schematic diagram of *P. putida* KT2440 central carbon metabolism and shinorine biosynthetic pathway. The initial biosynthetic step involves the synthesis of desmethyl 4-deoxygadusol (DDG) through sedoheptulose 7-phosphate (Balskus and Walsh, 2010; Pope et al., 2015). Desmethyl-4-deoxygadusol synthase (DDGS) catalyzes the production of DDG. Subsequently, *O*-methyltransferase (*O*-MT) transforms DDG to 4-deoxygadusol (4-DG). 4-DG incorporates glycine through an ATG-grasp ligase to yield mycosporine-glycine (MG). In the final step, MG is converted to shinorine by a non-ribosomal peptide synthetase (NRPS)-like enzyme (Balskus and Walsh, 2010; Portwich and Garcia-Pichel, 2003), which encompasses adenylation, thiolation, and thioesterase domains or by a D-Ala-D-Ala ligase. The adenylation domain plays a crucial role in attaching serine to the C1 position of mycosporine-glycine, generating shinorine. (B) Shinorine biosynthetic gene cluster (BGC) from *Anabaena variabilis* ATCC 29413 and *Nostoc punctiforme* ATCC 29133. Primers are indicated by red arrows. (C) Schematic diagram of plasmid pIY456 used for expression of shinorine BGC from *A. variabilis* ATCC 29413. This plasmid was used for production experiments in Fig. 3F. (D) Plasmid used for expression of shinorine BGC from *N. punctiforme* ATCC 29133. (E) Variation of plasmid shown in Fig. 3D with the introduction of a foreign RBS upstream the D-Ala-D-Ala ligase coding sequence. (F) Production of shinorine in *P. putida* KT2440 strains. Chromatogram obtained from *P. putida* (G) and extracted Helioguard™ (H). (I) Assigned ^{1}H and ^{13}C resonances for purified shinorine. (J) Correlations (^{1}H-^{1}H NOESY and ^{1}H-^{13}C HMBC) used to unambiguously assign all resonances for purified shinorine. *P. putida* KT2440 were grown in 5 mL M9 medium, and samples were extracted at 48 h. Error bars represent standard deviations from three biological replicates. SAM, *S*-adenosyl-*L*-methionine; SAH, *S*-adenosylhomocysteine. Other abbreviations are shown in Figure 1 caption.

To synthesize shinorine in *P. putida* KT2440, we began by amplifying the whole shinorine BGC from *A. variabilis* ATCC 29413 (MIBiG Accession Number: BGC0000427) and *N. punctiforme* ATCC 29133 (Balskus and Walsh, 2010; Qunjie and Ferran, 2011), keeping the intergenic regions unaltered. The amplified gene clusters were subsequently cloned into an RK-based vector under the control of a strong constitutive $P_{trc1\text{-}O}$ promoter (Fig. 3C,D). As the gene encoding D-Ala-D-Ala ligase appeared to be transcribed in the antisense direction, we also created another plasmid variant where we introduced a foreign RBS and changed the orientation of the gene (Fig. 3E). Despite several attempts, the production of shinorine in *P. putida* KT2440 could only be detected from the heterologous expression of shinorine BGC from *A. variabilis* ATCC 291413, yielding approximately 60 mg/L shinorine at 48 hr (Fig. 3F), with over 80% of shinorine accumulating in the supernatant.

The chromatographic analysis of the samples (Fig. 3G) showed that the shinorine peak (**1**) co-eluted with the shinorine peak obtained from the reference Helioguard™ standard (Fig. 3H). The accuracy of the mass spectrum was confirmed through LC-MS/MS (Supplementary Figure S3) and the results agreed with those previously reported (Kim et al., 2022). To further validate the chemical structure of shinorine, we purified the extract from a 1-L liquid culture and subjected it to nuclear magnetic resonance (NMR) spectroscopy. Correlations obtained via ^{1}H-^{1}H COSY, ^{1}H-^{1}H NOESY, ^{1}H-^{13}C HSQC and ^{1}H-^{13}C HMBC enabled the unambiguous assignment of all ^{1}H and ^{13}C resonances (Figure 3I, J and Supplementary Table S3). Observed resonances and assignments thereof were highly consistent with previous NMR data reported for shinorine (Miyamoto et al., 2014) (Supplementary Figures S4-S10). To our knowledge, this is the first report of shinorine production in *P. putida* KT2440.

2.4 Improvement of shinorine production titer by CRISPRi-mediated gene downregulation

To further improve the shinorine titer, we employed CRISPRi-mediated gene downregulation to suppress competing metabolic pathways and redirect carbon flux towards shinorine production. The use of CRISPRi holds the potential to improve the yield of desired metabolites by selectively repressing the expression of specific genes in metabolic pathways. This approach has proven successful in improving the production of various compounds, including isoprenol (Tian et al., 2019; Wang et al., 2022), free fatty acids (Fang et al., 2021), propane (Yunus et al., 2022), fatty alcohols (Kaczmarzyk et al., 2018), indigoidine (Banerjee et al., 2020), and many others (Zhao et al., 2021). In this study, we applied CRISPRi to downregulate a set of twenty-one genes involved in the central carbon metabolism and biosynthesis of *L*-serine and

glycine, two amino acids critical to the shinorine biosynthetic pathway (Fig. 4A). Catalytically inactive Cas9 protein was expressed in RSF1010 plasmid under the control of salicylic acid-inducible promoter (P_{nagA}) and the single guide RNA (sgRNA) was placed under the constitutive promoter P_{J23119} (Fig. 4B). This plasmid was coexpressed with the shinorine-producing RK2 plasmid.

Our findings demonstrated that knocking down the PP_1444 gene led to a significant increase in the shinorine titer. The *P. putida* KT2440 strain with downregulated PP_1444 produced approximately 400 mg/L shinorine in 72 hr, a 160% increase compared to the control strain (i.e., a strain with a nontarget sgRNA) (Fig. 4C). It is worth noting that the titer of the control strain shown here is approximately 3-fold higher at 48 hr compared to the strain shown in Fig. 3C. The presence of a CRISPRi plasmid appeared to influence the expression levels of DDGS, *O*-MT, ATP-grasp ligase, and NRPS (Supplementary Fig. S11). These changes might also be attributed to the heightened expression of the *aph* gene (Supplementary Fig. S12B), which may suggest that the copy number of the RK2 plasmid was altered in the presence of a second plasmid.

PP_1444 encodes quinoprotein glucose dehydrogenase, the enzyme responsible for the conversion of glucose to gluconate. In previous studies, it was observed that *P. putida* KT2440 tends to accumulate gluconate and 2-ketogluconate, and the accumulation of these two compounds is effectively eliminated by knocking out PP_1444 (Teresa et al., 2007). Interestingly, the knockout of PP_1444 has been associated with a growth defect in prior studies (Bentley et al., 2020). However, in our study, we did not observe any growth defects (Supplementary Fig. S13A). This discrepancy is likely attributable to the partial repression of PP_1444 achieved by CRISPRi (Fig. 4D), resulting in a decrease rather than a complete elimination of gluconate in both the supernatant and cell pellet fractions (Supplementary Fig. S13B, C). The decrease in gluconate levels both in cell pellet and supernatant fraction might indicate a potential redirection of carbon flux from glucose directly to the EDEMP cycle.

To investigate the impact of PP_1444 downregulation on central carbon metabolism, we perfomed metabolomics analyses on the control and PP_1444 strains at various sampling time points (Supplementary Fig. S13D-H). Although no discernible difference in the G6P pool was observed between the supernatant fractions of control (nontarget sgRNA) and PP_1444 strains (in fact, G6P levels were lower in the cell pellet fraction of PP_1444 for the first 48 hr), we consistently noted higher concentrations of 2/3PG and 6PG in both the supernatant and cell pellet fractions of the PP_1444 strain (Supplementary Fig. S13D,H). This might indicate that knocking down PP_1444 may enhance the availability of 6PG and 2/3PG, which can be beneficial for the

synthesis of glycine and *L*-serine. Interestingly, the S7P pool was lower in the cell pellet fraction of the PP_1444 strain for the first 48 hr. One plausible explanation is that the lower S7P levels in PP_1444 strain could be attributed to increased metabolic activity channeling S7P towards the shinorine biosynthetic pathway, fueled by the increased availability of glycine and *L*-serine substrates for shinorine biosynthesis. While these preliminary metabolomics findings offer insights into the metabolic alterations induced by PP_1444 downregulation, a comprehensive elucidation of the underlying mechanisms driving improvements of shinorine necessitates further dedicated study.

As the downregulation of PP_1444 appeared to be the only instance resulting in an increase in shinorine titer, we further investigated to verify the downregulation of other target genes. Among the 21 targeted genes, we observed that 10 were indeed downregulated, 3 exhibited no downregulation, and 8 could not be verified as the proteins were undetectable in both the sample and control strains (Fig. 4D). Of the three genes that were not downregulated (PP_1010, PP_2930, and PP_4677), with the exception of PP_4677, their respective dCas9 expression levels were low (Supplementary Fig. S12C) although the expression levels of the gentamicin selection markers were consistently maintained in these strains (Supplementary Fig. S12A). Recognizing the significance of flux from 6PG to 2KDPG (Fig. 1) as the major competing pathway for S7P synthesis, we designed additional sgRNAs targeting different regions within the coding sequence of PP_1010. Despite these efforts, no improvement in shinorine titer was observed. Sequencing analysis revealed mutations in the CRISPRi plasmid, resulting in a partial deletion of the CRISPRi plasmid – although the plasmid was still intact when cloned in *E. coli*. We hypothesized that since PP_1010 is an essential gene, as indicated by data retrieved from fit.genomics.lbl.gov, knocking down the PP_1010 could be detrimental to growth. Therefore, only *P. putida* KT2440 carrying the mutated CRISPRi plasmid (i.e., with no or low dCas9 expression) could dominate the population. This hypothesis is in agreement with the low expression level of dCas9 observed in our proteomics analysis. In the case of PP_4677, however, the dCas9 expression level was comparable to that of other strains. This leads us to speculate that the lack of downregulation observed in PP_4677 may be attributed to the inefficiency of the designed sgRNA of PP_4677. It underscores the importance of designing more effective sgRNAs to achieve efficient gene regulation in future experiments.

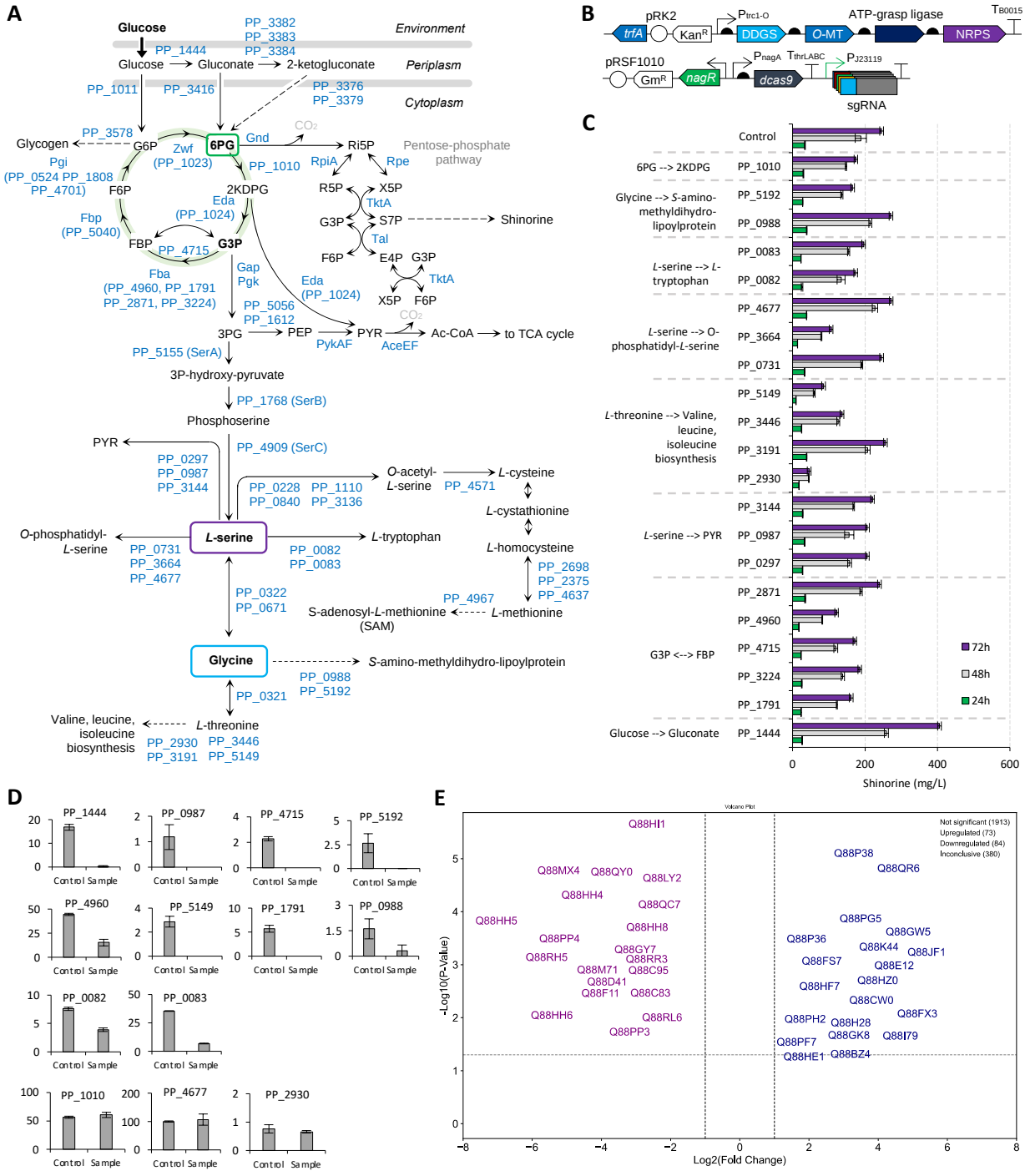

Figure 4. CRISPRi gene downregulation for improved shinorine production. (A) Schematic diagram of genes involved in 6PG, G3P, *L*-serine, glycine, and *S*-adenosyl-*L*-methionine (SAM) metabolism. (B) Schematic diagram of plasmids used for expression of shinorine biosynthetic genes and CRISPRi-mediated gene downregulation. (C) Shinorine titer produced by different strains targeting 21 genes. (D) Relative expression levels (y-axis; x10^6) of target genes in the control vs sample. (E) Volcano plot depicting top 20 downregulated (purple) and upregulated (navy) genes in the

PP_1444 strain. The dashed horizontal line represents statistical significance threshold ($P \leq 0.05$). All strains were cultivated in 5 mL M9 medium. Error bars represent standard deviation from three biological replicates.

Upon further investigation, in addition to PP_1444, we found that approximately 83 other genes were unexpectedly significantly downregulated in the PP_1444 strain (Fig. 4E, Supplementary Table S4). Among them, proteins involved in the metabolism of gluconate into 2-ketogluconate and 6PG (Fig. 4A), such as Q88HH4, Q88HH5, and Q88HH6 (gluconate 2-dehydrogenase, encoded by PP_3384, PP_3383, and PP_3382, respectively), as well as Q88HI1 (ketogluconate-6-P-reductase, encoded by PP_3376) and Q88HH8 (2-ketogluconate epimerase, encoded by PP_3379), were downregulated. Phosphoglucomutase (Q88GY7, encoded by PP_3578), an enzyme responsible for glycogen biosynthesis from G6P, also appeared to be downregulated. This may redirect G6P pool for the synthesis of 6PG (Fig. 4A). Additionally, *L*-serine dehydratase (Q88P66, encoded by PP_0987), which is involved in the conversion of *L*-serine to pyruvate, was also downregulated. This might preserve *L*-serine pool for shinorine biosynthesis. Interestingly, downregulating PP_0987 alone did not improve the shinorine titer (Fig. 4C). In addition to massive, unexpected gene downregulation, we found 73 genes were upregulated in PP_1444 strain (Fig. 4E, Supplementary Table S5). For example, 5-methyltetrahydropteroyltriglutamate-homocysteine methyltransferase (Q88JF1, encoded by PP_2698), was upregulated by 28-fold. This enzyme may be responsible for maintaining *L*-methionine synthesis used for biosynthesis of *S*-adenosyl-*L*-methionine (SAM), a methyl donor for *O*-methyltransferase.

These results may demonstrate that the downregulation of PP_1444 not only reduces the accumulation of gluconate but also has far-reaching effects on the expression of multiple genes in *P. putida* KT2440. Many of the listed proteins appear to be involved in various metabolic pathways, including amino acid and central carbon metabolism. Their direct roles in shinorine production are not clear. While some of these gene expression changes align with our goal of increasing shinorine production by redirecting carbon flux and preserving critical metabolites, others remain unexplained and require further investigation. Nevertheless, these findings highlight the potential of CRISPRi as a valuable tool for metabolic engineering and the production of desired compounds in microbial hosts, offering promising avenues for further optimization and enhancing the yield of shinorine and other valuable metabolites in biotechnological applications.

2.5 Pathway optimization through refining promoter usage and altering the strength of ribosome binding sites

In tandem with CRISPRi-mediated gene downregulation approach, we sought to improve the shinorine titer by refining the design of the genetic constructs, including optimizing promoter usage, and altering the strength of ribosome binding sites. Previous studies have demonstrated the effectiveness of adjusting RBS strength to enhance metabolite production (Jeschek et al., 2017; Jones et al., 2015; Rao et al., 2024; Yunus et al., 2020; Yunus and Jones, 2018). However, constructing plasmids for biosynthetic pathways involving multiple genes can be labor-intensive. To streamline this process, we adopted a modular linker-based plasmid construction method (Storch et al., 2015) to facilitate the creation of plasmid constructs with various RBSs, thereby tuning the expression levels of proteins involved in the shinorine pathway (Fig. 5A).

By employing two distinct promoters (P_{BAD} and $P_{trc1\text{-}O}$) and restructuring the shinorine BGC into either one or two transcriptional units, coupled with variations in RBSs, we successfully assembled twenty-one different plasmids (Fig. 5B). This combinatorial approach led to a significant increase in shinorine production, elevating it from 100 mg/L (Fig. 5C, JBx_250483, represented by the white bar) to approximately 467 mg/L shinorine (Fig. 5C, JBx_250497, represented by the black bar) within a 72-hr post inoculation.

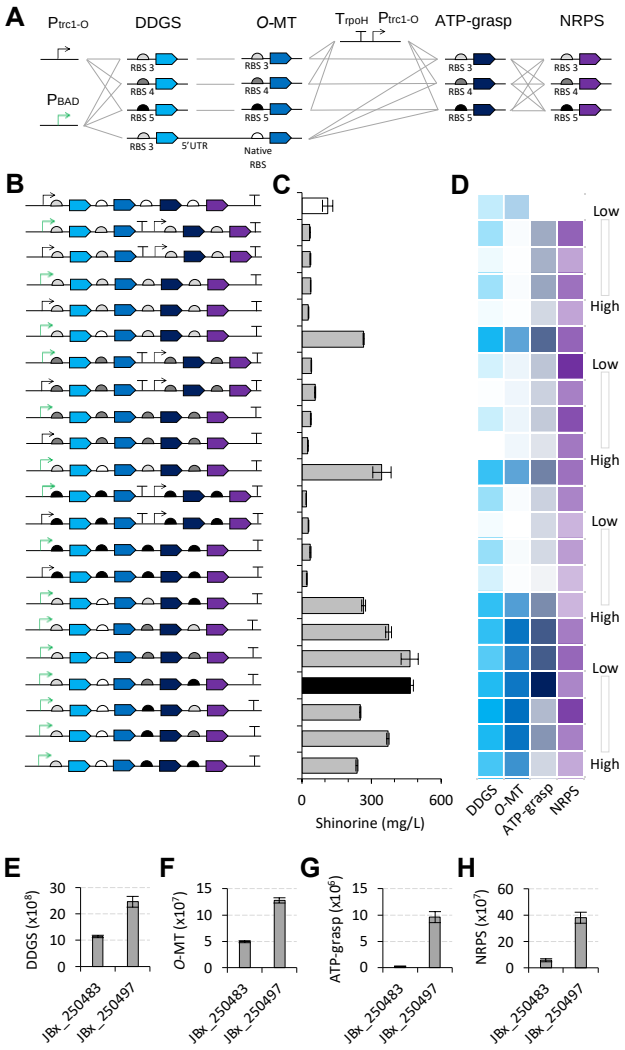

Figure 5. Improvement of shinorine production by RBS optimization. (A) Illustration of combinatorial modular plasmid assembly consisting of promoters and genes assembled to different RBS. Two types of promoters and three different RBS elements were used. (B) Schematic diagram of twenty-one different shinorine-producing plasmids. (C) Shinorine titers from strains carrying plasmid shown in Fig. 5B. White bar and black bar charts represent JBx_250483 and JBx_250497 strain, respectively. (D) Heatmap of shotgun proteomics analysis of DDGS, *O*-MT, ATP-grasp ligase, and NRPS. Expression levels of DDGS (E), *O*-MT (F), ATP-grasp ligase (G), and NRPS (H) from the control strain (JBx_250483) vs the highest shinorine producing strain (JBx_250497). Samples were grown in 5 mL of M9 minimal medium. Shinorine was extracted from the whole liquid culture at 72 hr. Error bars represent standard deviations from three biological replicates.

Our shotgun proteomics analysis revealed that manipulating promoters and RBSs proved to be a viable strategy for enhancing the expression levels of shinorine pathway proteins (Fig. 5D). The arabinose-inducible promoter P_{BAD} appeared to outperform the constitutive $P_{trc1\text{-}O}$ promoter. Substituting the native RBS with foreign RBS sequences, except for the native *O*-MT

RBS, resulted in a significant increase in protein expression levels. By employing a foreign RBS, we achieved substantial improvements in the expression levels of DDGS, *O*-MT, ATP-grasp ligase, and NRPS in JBx_250497, with improvements of 2.1-fold, 2.6-fold, 40.5-fold, and 6.7-fold, respectively, compared to the original strain (JBx_250483) (Fig. 5E-H).

To discern the enzyme(s) with the most significant impact on shinorine production, we performed a multiple linear regression analysis. The Ordinary Least Squares (OLS) regression results indicate that the expression levels of *O*-MT and ATP-grasp ligase carry considerable statistical significance in predicting shinorine titer, whereas DDGS and NRPS do not appear to have a significant effect in this model (Supplementary Table S6). This may imply that further improvements in the expression levels of *O*-MT and ATP-grasp ligase could lead to a more substantial increase in the shinorine titer. However, having robustly explored the available permutations of RBS variations, we found that optimizing these two enzyme's expression levels beyond a certain point did not yield significant improvements in shinorine production (Supplementary Fig. S14). Therefore, while *O*-MT and ATP-grasp ligase play a crucial role in predicting shinorine titer, there may be other factors or pathways that need to be considered for further enhancement.

2.6 Glycine and *L*-serine supplementation further improves shinorine production

Following the successful implementation of CRISPRi-mediated gene downregulation and the refinement of genetic constructs, we then combined the two strategies to further improve shinorine production. We used the highest shinorine producing strain (JBx_250497) as the base strain and co-transformed it with a CRISPRi plasmid harboring PP_1444 sgRNA or nontarget sgRNA (Fig. 6A). The PP_1444 strain produced approximately 524 mg/L shinorine at 66 hr while the control nontarget strain produced approximately 365 mg/L shinorine (Supplementary Fig. S15). The glucose consumption profiles indicate that glucose was completely in both samples after 42 hr. No significant growth and shinorine production were observed after 66 hr. These results might imply that the glucose supply was limiting the shinorine production under the tested condition.

To increase the supply of glucose, we added 20 g/L of glucose at 18 hr. Upon the addition of extra glucose, the PP_1444 strain produced approximately 723 mg/L of shinorine at 66 hr (Fig. 6B). The shinorine titer peaked at 902 mg/L at 90 hr. To explore if another glucose supplementation would further improve the titer, we added an extra 20 g/L of glucose at 42 hr (Fig. 6C) The additional glucose did not improve the final titer, indicating that another factor was potentially limiting the shinorine production.

The shinorine biosynthetic pathway involves the incorporation of two amino acids, glycine and *L*-serine. Glycine and *L*-serine are incorporated into the shinorine through specific enzymatic reactions (Fig. 4A). The ATP-grasp ligase, a key enzyme in the shinorine biosynthetic pathway, facilitates the incorporation of glycine into 4-deoxygadusol to form mycosporine-glycine, which is a precursor of shinorine. Subsequently, an NRPS-like enzyme attaches a serine moiety to mycosporine-glycine, resulting in the formation of shinorine. Considering the role of these amino acids in shinorine biosynthesis, we hypothesized that their external supplementation could potentially alleviate any metabolic bottleneck due to limited intracellular availability, thereby enhancing the overall production of shinorine.

To test this hypothesis, we conducted a series of fermentation experiments of PP_1444 and nontarget strains (Fig. 6D) with supplementation of glycine and *L*-serine. The supplementation of glycine and *L*-serine resulted in a marked increase in shinorine production, both in the PP_1444 and nontarget strains (compared Fig. 6E and 6B). For the PP_1444 strain, the shinorine titer increased sharply within the first 66 hr and then continued to steadily increase up to 1,134 mg/L at 114 hr (Fig. 6E). Approximately 1.7 g/L of glucose remained in the liquid cultures at 66 hr. To further improve the shinorine titer, we added an extra 20 g/L of glucose at 42 hr (Fig. 6F). Here, we observed a sharp increase of shinorine titer over 114 hr. The highest shinorine titer of 1,601 mg/L was achieved at 114 hr from the PP_1444 strain, where the strain completely consumed the glucose. In summary, without glycine and *L*-serine supplementation, we achieved a final titer, productivity, and yield of 900 mg/L, 10 mg/L/h, and 22.5 mg/g glucose, respectively. With the addition of glycine and *L*-serine, these metrics increased to 1,601 mg/L, 14 mg/L/h, and 26 – 28.35 mg/g glucose.

While these results mark a notable enhancement over the initial production levels and highlight the importance of glycine and *L*-serine in shinorine biosynthesis, relying on amino acid supplementation for large-scale production is not a feasible solution. Consequently, further genetic alterations are imperative to improve *de novo* biosynthesis of glycine and *L*-serine. Our CRISPRi studies have pinpointed genes potentially involved in glycine and *L*-serine metabolism. However, the results indicated that none of the downregulated genes associated with glycine and *L*-serine metabolism appeared to improve shinorine titer. This was rather expected, given that many reactions in glycine and *L*-serine metabolism involve more than one gene (Fig. 4A). While single-gene downregulation by CRISPRi was verified by shotgun proteomics, compensatory mechanisms involving other enzymes likely mitigated the impact of individual gene knockdowns. To overcome this challenge, future efforts must explore the synergistic effects of multiplexed CRISPRi, facilitating simultaneous knockdowns of multiple genes. This strategic approach not

only promises a more profound impact on target pathways, but also presents an avenue for deciphering the dynamics of metabolic networks, ultimately optimizing them for improved shinorine production.

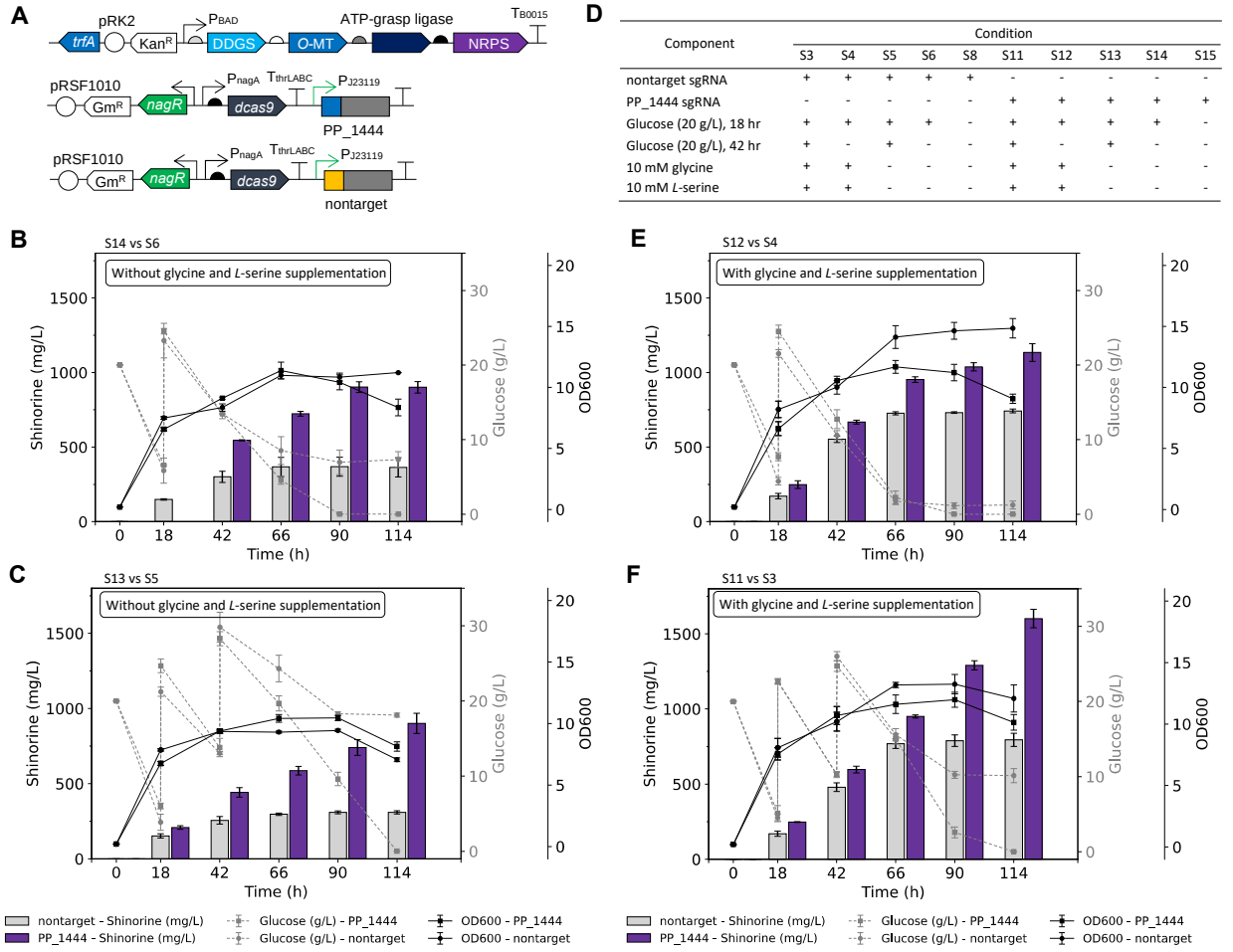

Figure 6. Effects of glycine and *L*-serine supplementation on shinorine production. (A) Schematics of genetics constructs used in the study. *P. putida* KT2440, carrying the shinorine biosynthetic pathway plasmid (JBx_250497), was transformed with a CRISPRi plasmid containing either PP_1444 sgRNA (JBx_249619) or nontarget sgRNA (JBx_249575). (B,C) Comparison of shinorine production, glucose consumption, and growth profiles over a 114-hour period without glycine and *L*-serine supplementation. (D) Experimental conditions used in B, C, E, and F. (E,F) Comparison of shinorine production, glucose consumption, and growth profiles over a 114-hour period with glycine and *L*-serine supplementation. All strains were cultivated in 25 mL M9 medium containing 20 g/L glucose with a starting OD600 of 0.1. At 4 hr post inoculation, cultures were induced with 0.2% *L*-arabinose, with or without the addition of 10 mM equimolar concentration of glycine and *L*-serine. At 18 hr, all cultures received an additional 20 g/L glucose. For samples in (D) and (F), an extra 20 g/L glucose was introduced to the cultures at the 42-hr time point. (Heberle et al., 2015) Error bars represent standard deviations from three biological replicates.

Following the extraction of samples from the whole liquid cultures, we also extracted shinorine from different fractions. The results unveiled that shinorine was found exclusively in the supernatant in the control strain (nontarget sgRNA) whereas for the PP_1444 strain, 91% and 9% shinorine was found in the supernatant and cell pellet, respectively (Fig. 7, Supplementary Fig. S16). To our knowledge, a specific *P. putida* transporter for shinorine is currently not known. However, our shotgun proteomics analysis revealed that the expression of several ABC efflux systems, transporters, and outer membrane efflux proteins was altered in the PP_1444 strain (Supplementary Table S4 and S5). These findings hint at the potential involvement of transporters in facilitating the export or import of shinorine in *P. putida* KT2440. However, further in-depth investigations are required to elucidate the precise mechanism and identify the specific transporter responsible for these transport processes.

From a biotechnological downstream processing perspective, the exclusive secretion of shinorine to the supernatant added significance to the use of *P. putida* KT2440 as a microbial platform for shinorine production. When the shinorine accumulates in the liquid medium rather than within the cells, it has several significant advantages for industrial biotechnology. Products in the supernatant can be harvested more easily as there is no need for cell disruption which simplifies the downstream processing and reduces costs (Ying Wang et al., 2019). It might also require less rigorous purification steps, which can be advantageous from a cost perspective. Additionally, if the product is secreted into the medium, the process could be adapted to a continuous production system where the product is continuously harvested while the culture is maintained. Accumulation of products within the cells can often lead to stress and eventual cell death (Cray et al., 2015). Secretion avoids this issue, maintaining cell viability and potentially increasing the overall yield of shinorine.

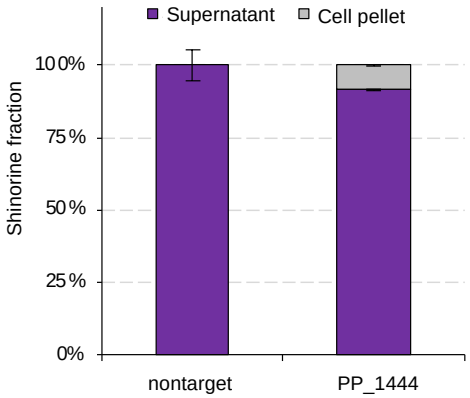

Fig. 7. Fraction of shinorine found in supernatant and cell pellet measured at 114 hr from samples in Fig. 6F. Error bars represent standard deviations from three biological replicates.

3. Materials and Methods

3.1 Strains, plasmids, media, and growth conditions

E. coli XL 1-Blue strain (Thermo Fisher Scientific) was used to propagate all the plasmids used in the study. The strain was routinely cultivated in lysogeny broth (LB) medium (LB Broth, Sigma Aldrich), 37 °C, 180 rpm, and supplemented with appropriate antibiotic(s) (final concentration: gentamicin 10 µg/mL, and kanamycin 50 µg/mL). Plasmids were constructed using a modular plasmid assembly method, namely Biopart Assembly Standard Idempotent Cloning (BASIC) (Storch et al., 2015) with modification.

Self replicating plasmids (RK2 and RSF1010-based plasmids) were transformed into *Pseudomonas putida* KT2440 by electroporation. The electroporation procedure was modified from (Choi et al., 2006). Briefly, one fresh colony of *P. putida* KT2440 was inoculated into 5 mL of LB and incubated for overnight at 30 °C, 200 rpm. Overnight culture was centrifuged for 1 min at 13,000 x *g*, washed three times with 1 mL 10% glycerol, and resuspended in 500 µL of 10% glycerol at room temperature. Electroporation was performed by adding approximately 100 ng DNA into 100 µL cell aliquot and shocked with Bio-Rad GenePulser II (USA) using 1 mm cuvette (1.8k kV, 200 Ω). After electroporation, a volume of 1 mL LB media was added into the cuvette and the cell mixtures were transferred into a fresh 1.5 mL microtube. For cell recovery, the cell mixtures were allowed to grow at 30 °C, 200 rpm, for 1 h. After incubation, 20 µL of cell mixtures was plated onto a selective agar plate containing appropriate antibiotic and incubated at 30 °C overnight. Plasmids used in this study are listed in Supplementary Table S7.

P. putida KT2440 seed cultures were inoculated from single colonies and grown in 5 mL LB medium at 30 °C, 180 rpm, overnight. Unless stated otherwise, 100 µL of the overnight cultures were transferred into 5 mL of M9 minimal medium (Banerjee et al., 2024), and incubated at 30 °C, 180 rpm, overnight. This process was repeated one more time to allow complete adaptation to M9 medium. For shinorine production, unless otherwise indicated, cell cultures were inoculated at an OD_{600} of 0.2 in 5 mL of M9 medium supplemented with 2% glucose and appropriate antibiotics (kanamycin 50 mg/L, gentamicin 10 mg/L), and induced with 0.2% (w/v) *L*-arabinose at 4 hr post-inoculation.

3.2 Routine shinorine extraction and analysis

For routine shinorine analysis from a whole liquid culture, 100 µL of liquid culture was mixed with 250 µL of methanol and 125 µL of chloroform. The resulting mixture was vortexed for 5 min at 3,000 rpm. Next, 125 µL of ultrapure water and 100 µL of chloroform were added and the samples were re-vortexed for 5 min at 3000 rpm followed by centrifugation for 1 min at 13,000

x g. Shinorine was then sampled from the top aqueous layer and measured using a NanoDrop™ 2000/2000c Spectrophotometers at 334 nm. To determine the concentration of shinorine in the sample, serially diluted purified shinorine standards were prepared and the concentration was determined using the Beer-lambert law with ε = extinction coefficient of shinorine (ε = 44,700 M^{-1} cm^{-1}). (Llewellyn et al., 2020; Wada et al., 2015).

For the analysis of extracellular shinorine, 100 µL of liquid culture was centrifuged for 5 min at 13,000 x g, and shinorine was measured from the supernatant without extraction. For the analysis of intracellular shinorine, 100 µL of liquid culture was centrifuged for 5 min at 13,000 x g. The supernatant was removed, and the cell pellet was washed three times with 500 µL of ultrapure water. Finally, the cell pellet was resuspended in 100 µL of ultrapure water and mixed with 250 µL of methanol and 125 µL of chloroform, following the extraction method described above for the whole liquid culture.

3.3 Construction of CRISPRi plasmids

For CRISPRi-mediated gene downregulation, single guide RNAs (sgRNAs) with 22 nucleotide sequences were designed using the web tool CRISPOR (Concordet and Haeussler, 2018) to target the non-template strand with NGG protospacer adjacent motif (PAM) sequence. A pair of complementary DNA oligos was ordered from Integrated DNA Technologies, hybridized at 95 °C for 10 min, and cooled down to room temperature in a heating block. Hybridized oligo was digested with *Bsa*I (New England Biolabs) and ligated to *PaqC*I-digested pIY993 plasmid (JBx_249165). The resulting plasmid was digested with *Bsa*I and cloned into pIY989 plasmid (JBx_249567). Hybridized oligos used for CRISPRi-mediated gene downregulation are listed in Supplementary Table S8.

3.4 Fluorescence measurement

Fluorescence measurement was done using a flow cytometer, 2 mL of LB media was inoculated with overnight culture (0.1% v/v) and supplemented with appropriate antibiotics. After 24 hr of incubation, 1-3 µL of samples was added to 150 µL 1X phosphate buffered saline. Single-cell RFP and GFP fluorescence from at least 30,000 cells was immediately recorded using a BD C6 Accuri flow cytometer (BD Bioscience). GFP and RFP fluorescence was measured using FL1 and FL4 detector, respectively. Protein fluorescent level was determined by taking the average of the fluorescence distribution.

3.5 Shinorine standard preparation

Shinorine-producing strain was cultivated in 250 mL M9 medium in a 1-L flask with a starting OD_{600} 0.2. At 48 hr post inoculation, sample was centrifuged at 4 °C, 4,500 x g for 30 min. To concentrate and desalt shinorine from the culture supernatant, the supernatant was loaded onto a HyperCarb 2G SPE column (Thermo Scientific), washed with 10 mL of 5% acetonitrile, and eluted with 10 mL of 80% aceteonitrile. The eluent was evaporated to dryness on a LabConco SpeedVac. The dried SPE elution was then reconstituted in MilliQ water and semi-purified using an Agilent 1260 HPLC system equipped with a Machery-Nagel Nucleosil 100-10 SB strong anion exchange column (250 mm x 4.6 mm, 10 µm particle size) operating at a flow rate of 1 mL/min using an isocratic mobile phase composed of 25 mM LC-MS grade ammonium bicarbonate (Fisher Scientific). Fractions were manually collected by monitoring the absorbance of the shinorine chromophore (λ = 334 nm). The observed retention time for shinorine was approximately 12.4 minutes. Collected fractions were then evaporated to dryness on a LabConco SpeedVac.

Dried fractions from anion exchange semi-purification were reconstituted in water and injected onto an Agilent 1260 HPLC system equipped with a Thermo HyperCarb column (150 mm x 4.6 mm, 5 µm particle size) operating at 1.5 mL/min using the following gradient (A = 0.3% ammonium formate pH 9.0, B = acetonitrile): 0 min 2% B, 20 min 15% B, 26 min 50% B, 27-33 min 90% B, 35-40 min 2% B. Fractions were manually collected by monitoring the absorbance of the shinorine chromophore (λ = 334 nm). The observed retention time for shinorine was approximately 9.2 minutes. Fractions containing shinorine were then flash frozen in liquid nitrogen and placed on a LabConco lyophilizer. The dried fractions were reconstituted in water, frozen, and lyophilized three times to volatilize residual ammonium formate. The resulting dried solid of purified shinorine was then used for characterization by NMR spectroscopy.

3.6 NMR spectroscopy of purified shinorine

Approximately 4.6 mg of purified shinorine was dissolved in 400 µL methanol-d_4 with 0.03% trimethylsilane (>99.8% atom % D; Sigma-Aldrich). NMR spectra were obtained on a Bruker Avance NEO 500 MHz equipped with a 5 mm ^{1}H/BB iProbe. Samples were held at 298 K during acquisition. Standard Bruker pulse sequences were used for each of the following experiments: ^{1}H, ^{13}C, ^{1}H-^{1}H COSY, ^{1}H-^{1}H NOESY (750 ms mixing time), ^{1}H-^{13}C HSQC, and ^{1}H-^{13}C HMBC. Spectra were recorded using the Bruker TopSpin 4.0.6 software and analyzed using MestReNova 14.3.2. Chemical shifts (δ, ppm) were referenced internally to trimethylsilane.

3.7 Proteomics analysis

Protein was extracted from cell pellets and tryptic peptides were prepared by following established proteomic sample preparation protocol (Chen et al., 2023) Briefly, cell pellets were resuspended in Qiagen P2 Lysis Buffer (Qiagen, Germany) to promote cell lysis. Proteins were precipitated with addition of 1 mM NaCl and 4 x vol acetone, followed by two additional washes with 80% acetone in water. The recovered protein pellet was homogenized by pipetting mixing with 100 mM ammonium bicarbonate in 20% methanol. Protein concentration was determined by the DC protein assay (BioRad, USA). Protein reduction was accomplished using 5 mM tris 2-(carboxyethyl)phosphine (TCEP) for 30 min at room temperature, and alkylation was performed with 10 mM iodoacetamide (IAM; final concentration) for 30 min at room temperature in the dark. Overnight digestion with trypsin was accomplished with a 1:50 trypsin:total protein ratio. The resulting peptide samples were analyzed on an Agilent 1290 UHPLC system coupled to a Thermo Scientific Orbitrap Exploris 480 mass spectrometer for discovery proteomics (Chen et al., 2020). Briefly, peptide samples were loaded onto an Ascentis® ES-C18 Column (Sigma–Aldrich, USA) and were eluted from the column by using a 10 minute gradient from 98% solvent A (0.1 % FA in H2O) and 2% solvent B (0.1% FA in ACN) to 65% solvent A and 35% solvent B. Eluting peptides were introduced to the mass spectrometer operating in positive-ion mode and were measured in data-independent acquisition (DIA) mode with a duty cycle of 3 survey scans from m/z 380 to m/z 985 and 45 MS2 scans with precursor isolation width of 13.5 m/z to cover the mass range. DIA raw data files were analyzed by an integrated software suite DIA-NN (Demichev et al., 2020). The database used in the DIA-NN search (library-free mode) was *P. putida* KT2440 latest Uniprot proteome FASTA sequences plus the protein sequences of the heterologous proteins and common proteomic contaminants. DIA-NN determines mass tolerances automatically based on first pass analysis of the samples with automated determination of optimal mass accuracies. The retention time extraction window was determined individually for all MS runs analyzed via the automated optimization procedure implemented in DIA-NN. Protein inference was enabled, and the quantification strategy was set to Robust LC = High Accuracy. Output main DIA-NN reports were filtered with a global FDR = 0.01 on both the precursor level and protein group level. The Top3 method, which is the average MS signal response of the three most intense tryptic peptides of each identified protein, was used to plot the quantity of the targeted proteins in the samples (Ahrné et al., 2013; Silva et al., 2006). The generated mass spectrometry proteomics data have been deposited to the ProteomeXchange Consortium via the PRIDE partner repository with the dataset identifier PXD050908 (Perez-Riverol et al., 2022).

3.8 Metabolomics analysis

The LC-MS/MS analysis was conducted on a Kinetex XB-C18 column (100-mm length, 3.0-mm internal diameter, and 2.6-µm particle size; Phenomenex, Torrance, CA USA) using a 1260 Infinity HPLC system (Agilent Technologies, Santa Clara, CA, USA). A sample injection volume of 2 µL was used throughout. The sample tray and column compartment were set to 6 and 20 °C, respectively. The mobile phase was composed of 10 mM ammonium formate and 0.2 % formic acid (Sigma-Aldrich, St. Louis, MO, USA) in water (solvent A) and 10 mM ammonium formate and 0.2 % formic acid in 90% acetonitrile and 9.8% water (solvent B). Shinorine was separated via gradient elution under the following conditions: linearly decreased from 90 %B to 70 %B in 4 min, held at 70 %B for 1.5 min, linearly decreased from 70 %B to 40 % B in 0.5 min, held at 40 %B for 2.5 min, linearly increased form 40 %B to 90 %B in 0.5 min, held at 90 %B for 2 min. The flow rate was held at 0.6 mL/min for 6.5 min, linearly increased from 0.6 mL/min to1 mL/min in 0.5 min, held at 1 mL/min for 4 min. The total LC run time was 11 min. The HPLC system was coupled to an Agilent Technologies 6520 quadrupole time-of-flight mass spectrometer (for LC-QTOF-MS). The QTOF-MS was tuned with Agilent Technologies ESI-L Low concentration tuning mix in the range of 50-1700 m/z. Drying and nebulizing gases were set to 12 L/min and 25 lb/in^2, respectively, and a drying-gas temperature of 350 °C was used throughout. Electrospray ionization was conducted in the positive ion mode (for $[M + H]^+$ ions) and a capillary voltage of 3500 V was utilized. The fragmentor, skimmer, and OCT 1 RF Vpp voltages were set to 100 V, 50 V, and 250 V, respectively. For targeted MS/MS, a precursor ion of 333.12942 m/z was selected for collision induced dissociation at a collision energy of 30 eV with a narrow isolation width of 1.3 m/z. The acquisition rate was 1 spectra/s. The data acquisition range was from 40-1100 m/z. Data acquisition (Workstation B.08.00) and processing (Qualitative Analysis B.06.00) were conducted via Agilent Technologies MassHunter software.

3.9 Carbon flux distribution prediction by genome-scale metabolic models

Genome-scale metabolic models were used to predict the flux sum (Chung and Lee, 2009) around 6-phosphogluconate. Metabolic flux distribution in a glucose minimal medium was first predicted by parsimonious flux balance analysis (Lewis et al., 2010), and the sum of all incoming or outgoing fluxes around 6-phosphogluconate was calculated and normalized by the glucose uptake rate for each model.

4. Conclusion

Growing interest in sourcing a sustainable and environmentally friendly sunscreen has motivated scientists to produce shinorine, a naturally occurring compound with UV-absorbing

properties, in microbes. Our study provides a comprehensive approach for engineering *Pseudomonas putida* KT2440 as an efficient chassis for shinorine production. Comprehensive review of metabolic flux distribution from different microbes pinpoint *P. putida* KT2440 as a potential host for shinorine production. By leveraging synthetic biology approaches and metabolic engineering strategies, we have significantly increased shinorine yield and productivity CRISPRi-mediated gene downregulation, particularly targeting the PP_1444 gene, significantly improved shinorine production compared to the first-engineered strain. Proteomics analysis shows downregulation of PP_1444 has far-reaching effects on the expression of multiple genes in *P. putida* KT2440. Refinement of genetic design, promoter usage, and ribosome binding sites also contributed to the titer improvement. Feeding studies indicate that the supply of two critical amino acids, *L*-serine and glycine, might be the limiting factor in shinorine biosynthesis. The final titer, productivity, and yield of 900 mg/L, 10 mg/L/h, and 22.5 mg/g glucose (without glycine and *L*-serine supplementation) and 1,601 mg/L, 14 mg/L/h, and 26 – 28.35 mg/g glucose (with glycine and *L*-serine supplementation), respectively, represent a substantial improvement over the initial production levels and surpass achievements of earlier studies. Additionally, the exclusive secretion of shinorine into the culture medium offers advantages for downstream processing in industrial applications. These findings underscore the potential of *P. putida* KT2440 as a microbial platform to produce valuable natural compounds. Through continued optimization and scale-up efforts, our work paves the way for the commercialization of shinorine as a bio-based alternative in the sunscreen industry.

5. Acknowledgement

We thank Drs. Hasan Celik, Raynald Giovine, and Pines Magnetic Resonance Center's Core NMR Facility (PMRC Core) for spectroscopic assistance. This material is based upon work supported by the Joint BioEnergy Institute (http://www.jbei.org), U.S. Department of Energy, Office of Science, Biological and Environmental Research Program under Award Number DE-AC02-05CH11231 with Lawrence Berkeley National Laboratory. The instruments used in this work were supported by the PMRC Core. Pacific Northwest National Laboratory portion is operated for the U.S. Department of Energy by Battelle under Contract DE-AC05–76RL01830. The United States Government retains a non-exclusive, paid-up, irrevocable, worldwide license to publish or reproduce the published form of this manuscript, or permit others to do so, for United States Government purposes. The views and opinions expressed by the authors do not necessarily reflect those of the United States Government or any of its agencies. The United States Government and its employees make no warranty, expressed or implied, regarding the

accuracy, completeness, or usefulness of any information, apparatus, product, or process disclosed, nor do they represent that the use of such information would not infringe privately owned rights.

6. Author Contributions

Conceptualization and design of the project: Yunus, Lee. Acquisition of data: Yunus, Hudson, Chen, Gin, Baidoo. Analysis and interpretation of data: Yunus, Hudson, Chen, Kim, Baidoo, Petzold, Lee. Drafting of manuscript: Yunus, Hudson, Chen, Kim, Baidoo, Petzold, Lee. Critical revision: Yunus, Hudson, Kim, Baidoo, Petzold, Adams, Simmons, Mukhopadhyay, Keasling, Lee. Funding acquisition: Adams, Simmons, Mukhopadhyay, Keasling, Lee. All authors contributed to and provided feedback on the manuscript. All authors read and approved the final manuscript.

7. Competing Interests

The authors declare no competing interests.

8. Supporting Information

Supplementary Figures and Supplementary Tables are available in a separate pdf file ("Supporting Information.pdf").

References

Ahrné, E., Molzahn, L., Glatter, T., Schmidt, A., 2013. Critical assessment of proteome-wide label-free absolute abundance estimation strategies. Proteomics 13, 2567–2578. https://doi.org/https://doi.org/10.1002/pmic.201300135

Aidelberg, G., Towbin, B.D., Rothschild, D., Dekel, E., Bren, A., Alon, U., 2014. Hierarchy of non-glucose sugars in Escherichia coli. BMC Syst Biol 8, 133. https://doi.org/10.1186/s12918-014-0133-z

Anderson, Jc., Dueber, J.E., Leguia, M., Wu, G.C., Goler, J.A., Arkin, A.P., Keasling, J.D., 2010. BglBricks: A flexible standard for biological part assembly. J Biol Eng 4, 1. https://doi.org/10.1186/1754-1611-4-1

Antoine, R., Locht, C., 1992. Isolation and molecular characterization of a novel broad-host-range plasmid from Bordetella bronchiseptica with sequence similarities to plasmids from

816 Gram-positive organisms. Mol Microbiol 6, 1785–1799.
817 https://doi.org/https://doi.org/10.1111/j.1365-2958.1992.tb01351.x
818 Aparicio, T., de Lorenzo, V., Martínez-García, E., 2019. Improved Thermotolerance of Genome-
819 Reduced Pseudomonas putida EM42 Enables Effective Functioning of the PL/cI857
820 System. Biotechnol J 14, 1800483. https://doi.org/https://doi.org/10.1002/biot.201800483
821 Aparicio, T., Nyerges, A., Martínez-García, E., de Lorenzo, V., 2020. High-Efficiency Multi-site
822 Genomic Editing of Pseudomonas putida through Thermoinducible ssDNA
823 Recombineering. iScience 23, 100946.
824 https://doi.org/https://doi.org/10.1016/j.isci.2020.100946
825 Bagdasarian, M.M., Amann, E., Lurz, R., Rückert, B., Bagdasarian, M., 1983. Activity of the
826 hybrid trp-lac (tac) promoter of Escherichia coli in Pseudomonas putida. Construction of
827 broad-host-range, controlled-expression vectors. Gene 26, 273–282.
828 https://doi.org/https://doi.org/10.1016/0378-1119(83)90197-X
829 Balskus, E.P., Walsh, C.T., 2010. The Genetic and Molecular Basis for Sunscreen Biosynthesis
830 in Cyanobacteria. Science (1979) 329, 1653–1656.
831 https://doi.org/10.1126/science.1193637
832 Banerjee, D., Eng, T., Lau, A.K., Sasaki, Y., Wang, B., Chen, Y., Prahl, J.-P., Singan, V.R.,
833 Herbert, R.A., Liu, Y., Tanjore, D., Petzold, C.J., Keasling, J.D., Mukhopadhyay, A., 2020.
834 Genome-scale metabolic rewiring improves titers rates and yields of the non-native product
835 indigoidine at scale. Nat Commun 11, 5385. https://doi.org/10.1038/s41467-020-19171-4
836 Banerjee, D., Yunus, I.S., Wang, X., Kim, Jinho, Srinivasan, A., Menchavez, R., Chen, Y., Gin,
837 J.W., Petzold, C.J., Martin, H.G., Magnuson, J.K., Adams, P.D., Simmons, B.A.,
838 Mukhopadhyay, A., Kim, Joonhoon, Lee, T.S., 2024. Genome-scale and pathway
839 engineering for the sustainable aviation fuel precursor isoprenol production in
840 Pseudomonas putida. Metab Eng 82, 157–170.
841 https://doi.org/https://doi.org/10.1016/j.ymben.2024.02.004
842 Becker, K., Hartmann, A., Ganzera, M., Fuchs, D., Gostner, J.M., 2016. Immunomodulatory
843 effects of the mycosporine-like amino acids shinorine and porphyra-334. Mar. Drugs 14,
844 119.
845 Bentley, G.J., Narayanan, N., Jha, R.K., Salvachúa, D., Elmore, J.R., Peabody, G.L., Black,
846 B.A., Ramirez, K., De Capite, A., Michener, W.E., Werner, A.Z., Klingeman, D.M.,
847 Schindel, H.S., Nelson, R., Foust, L., Guss, A.M., Dale, T., Johnson, C.W., Beckham, G.T.,
848 2020. Engineering glucose metabolism for enhanced muconic acid production in

849 Pseudomonas putida KT2440. Metab Eng 59, 64–75.
850 https://doi.org/https://doi.org/10.1016/j.ymben.2020.01.001
851 Bommareddy, R.R., Sabra, W., Maheshwari, G., Zeng, A.-P., 2015. Metabolic network analysis
852 and experimental study of lipid production in Rhodosporidium toruloides grown on single
853 and mixed substrates. Microb Cell Fact 14, 36. https://doi.org/10.1186/s12934-015-0217-5
854 Brink, D.P., Mierke, F., Norbeck, J., Siewers, V., Andlid, T., 2023. Expanding the genetic toolbox
855 of Rhodotorula toruloides by identification and validation of six novel promoters induced or
856 repressed under nitrogen starvation. Microb Cell Fact 22, 160.
857 https://doi.org/10.1186/s12934-023-02175-2
858 Calero, P., Jensen, S.I., Nielsen, A.T., 2016. Broad-Host-Range ProUSER Vectors Enable Fast
859 Characterization of Inducible Promoters and Optimization of p-Coumaric Acid Production in
860 Pseudomonas putida KT2440. ACS Synth Biol 5, 741–753.
861 https://doi.org/10.1021/acssynbio.6b00081
862 Chen, Y., Gin, J., Petzold, C., 2020. Discovery proteomic (DDA) LC-MS/MS data acquisition
863 and analysis. protocols.io. https://dx.doi.org/10.17504/protocols.io.bgbqjsmw.
864 Chen, Y., Gin, J.W., Wang, Y., de Raad, M., Tan, S., Hillson, N.J., Northen, T.R., Adams, P.D.,
865 Petzold, C.J., 2023. Alkaline-SDS cell lysis of microbes with acetone protein precipitation
866 for proteomic sample preparation in 96-well plate format. PLoS One 18, e0288102-.
867 Choi, K.-H., Kumar, A., Schweizer, H.P., 2006. A 10-min method for preparation of highly
868 electrocompetent Pseudomonas aeruginosa cells: Application for DNA fragment transfer
869 between chromosomes and plasmid transformation. J. Microbiol. Methods 64, 391.
870 Choi, Y.-H., Yang, D.J., Kulkarni, A., Moh, S.H., Kim, K.W., 2015. Mycosporine-Like Amino
871 Acids Promote Wound Healing through Focal Adhesion Kinase (FAK) and Mitogen-
872 Activated Protein Kinases (MAP Kinases) Signaling Pathway in Keratinocytes. Mar Drugs
873 13, 7055–7066. https://doi.org/10.3390/md13127056
874 Chung, B.K.S., Lee, D.-Y., 2009. Flux-sum analysis: a metabolite-centric approach for
875 understanding the metabolic network. BMC Syst Biol 3, 117. https://doi.org/10.1186/1752-
876 0509-3-117
877 Concordet, J.-P., Haeussler, M., 2018. CRISPOR: intuitive guide selection for CRISPR/Cas9
878 genome editing experiments and screens. Nucleic Acids Res 46, W242–W245.
879 https://doi.org/10.1093/nar/gky354
880 Cook, T.B., Rand, J.M., Nurani, W., Courtney, D.K., Liu, S.A., Pfleger, B.F., 2018. Genetic tools
881 for reliable gene expression and recombineering in Pseudomonas putida. J Ind Microbiol
882 Biotechnol 45, 517–527. https://doi.org/10.1007/s10295-017-2001-5

883 Cray, J.A., Stevenson, A., Ball, P., Bankar, S.B., Eleutherio, E.C.A., Ezeji, T.C., Singhal, R.S.,
884 Thevelein, J.M., Timson, D.J., Hallsworth, J.E., 2015. Chaotropicity: a key factor in product
885 tolerance of biofuel-producing microorganisms. Curr Opin Biotechnol 33, 228–259.
886 https://doi.org/https://doi.org/10.1016/j.copbio.2015.02.010
887 Damalas, S.G., Batianis, C., Martin-Pascual, M., de Lorenzo, V., Martins dos Santos, V.A.P.,
888 2020. SEVA 3.1: enabling interoperability of DNA assembly among the SEVA, BioBricks
889 and Type IIS restriction enzyme standards. Microb Biotechnol 13, 1793–1806.
890 https://doi.org/https://doi.org/10.1111/1751-7915.13609
891 De Bernardez, E.R., Dhurjati, P.S., 1987. Effect of a broad-host range plasmid on growth
892 dynamics of Escherichia coli and Pseudomonas putida. Biotechnol Bioeng 29, 558–565.
893 https://doi.org/https://doi.org/10.1002/bit.260290504
894 De Graaf, A.A., Striegel, K., Wittig, R.M., Laufer, B., Schmitz, G., Wiechert, W., Sprenger, G.A.,
895 Sahm, H., 1999. Metabolic state of Zymomonas mobilis in glucose-, fructose-, and xylose-
896 fed continuous cultures as analysed by 13C- and 31P-NMR spectroscopy. Arch Microbiol
897 171, 371–385. https://doi.org/10.1007/s002030050724
898 Demichev, V., Messner, C.B., Vernardis, S.I., Lilley, K.S., Ralser, M., 2020. DIA-NN: neural
899 networks and interference correction enable deep proteome coverage in high throughput.
900 Nat Methods 17, 41–44. https://doi.org/10.1038/s41592-019-0638-x
901 Dvořák, P., de Lorenzo, V., 2018. Refactoring the upper sugar metabolism of Pseudomonas
902 putida for co-utilization of cellobiose, xylose, and glucose. Metab Eng 48, 94–108.
903 https://doi.org/https://doi.org/10.1016/j.ymben.2018.05.019
904 Elmore, J.R., Furches, A., Wolff, G.N., Gorday, K., Guss, A.M., 2017. Development of a high
905 efficiency integration system and promoter library for rapid modification of Pseudomonas
906 putida KT2440. Metab Eng Commun 5, 1–8.
907 https://doi.org/https://doi.org/10.1016/j.meteno.2017.04.001
908 Fang, L., Fan, J., Luo, S., Chen, Y., Wang, C., Cao, Y., Song, H., 2021. Genome-scale target
909 identification in Escherichia coli for high-titer production of free fatty acids. Nat Commun
910 12, 4976. https://doi.org/10.1038/s41467-021-25243-w
911 Farinha, M.A., Kropinski, A.M., 1990. Construction of broad-host-range plasmid vectors for easy
912 visible selection and analysis of promoters. J Bacteriol 172, 3496–3499.
913 https://doi.org/10.1128/jb.172.6.3496-3499.1990
914 Hartmann, A.; Gostner, J.; Fuchs, J.; Chaita, E.; Aligiannis, N.; Skaltsounis, L.; Ganzera, M..,
915 2015. Inhibition of Collagenase by Mycosporine-like Amino Acids from Marine Sources.
916 Planta Med 81, 813–820. https://doi.org/10.1055/s-0035-1546105

Hüsken, L., Beeftink, R., de Bont, J., Wery, J., 2001. High-rate 3-methylcatechol production in Pseudomonas putida strains by means of a novel expression system. Appl Microbiol Biotechnol 55, 571–577. https://doi.org/10.1007/s002530000566

Itoh, Y., Haas, D., 1985. Cloning vectors derived from the Pseudomonas plasmid pVS1. Gene 36, 27–36. https://doi.org/https://doi.org/10.1016/0378-1119(85)90066-6

Jacobson, T.B., Adamczyk, P.A., Stevenson, D.M., Regner, M., Ralph, J., Reed, J.L., Amador-Noguez, D., 2019. 2H and 13C metabolic flux analysis elucidates in vivo thermodynamics of the ED pathway in Zymomonas mobilis. Metab Eng 54, 301–316. https://doi.org/https://doi.org/10.1016/j.ymben.2019.05.006

Jeschek, M., Gerngross, D., Panke, S., 2017. Combinatorial pathway optimization for streamlined metabolic engineering. Curr Opin Biotechnol 47, 142–151. https://doi.org/https://doi.org/10.1016/j.copbio.2017.06.014

Jin, C., Kim, S., Moon, S., Jin, H., Hahn, J.-S., 2021. Efficient production of shinorine, a natural sunscreen material, from glucose and xylose by deleting HXK2 encoding hexokinase in Saccharomyces cerevisiae. FEMS Yeast Res. 21, foab053.

Jin, H., Kim, S., Lee, D., Ledesma-Amaro, R., Hahn, J.-S., 2023. Efficient production of mycosporine-like amino acids, natural sunscreens, in Yarrowia lipolytica. Biotechnology for Biofuels and Bioproducts 16, 162. https://doi.org/10.1186/s13068-023-02415-y

Johnson, J. V, Dick, J.T.A., Pincheira-Donoso, D., 2022. Marine protected areas do not buffer corals from bleaching under global warming. BMC Ecol Evol 22, 58. https://doi.org/10.1186/s12862-022-02011-y

Jones, J.A., Toparlak, Ö.D., Koffas, M.A.G., 2015. Metabolic pathway balancing and its role in the production of biofuels and chemicals. Curr Opin Biotechnol 33, 52–59. https://doi.org/https://doi.org/10.1016/j.copbio.2014.11.013

Kaczmarzyk, D., Cengic, I., Yao, L., Hudson, E.P., 2018. Diversion of the long-chain acyl-ACP pool in Synechocystis to fatty alcohols through CRISPRi repression of the essential phosphate acyltransferase PlsX. Metab Eng 45, 59–66. https://doi.org/https://doi.org/10.1016/j.ymben.2017.11.014

Kim, S., Park, B.G., Jin, H., Lee, D., Teoh, J.Y., Kim, Y.J., Lee, S., Kim, S.-J., Moh, S.H., Yoo, D., Choi, W., Hahn, J.-S., 2023. Efficient production of natural sunscreens shinorine, porphyra-334, and mycosporine-2-glycine in Saccharomyces cerevisiae. Metab Eng 78, 137–147. https://doi.org/https://doi.org/10.1016/j.ymben.2023.05.009

Kim, S.-R., Cha, M., Kim, T., Song, S., Kang, H.J., Jung, Y., Cho, J.-Y., Moh, S.H., Kim, S.-J., 2022. Sustainable Production of Shinorine from Lignocellulosic Biomass by Metabolically

Engineered Saccharomyces cerevisiae. J Agric Food Chem 70, 15848–15858. https://doi.org/10.1021/acs.jafc.2c07218

Kohlstedt, M., Wittmann, C., 2019. GC-MS-based 13C metabolic flux analysis resolves the parallel and cyclic glucose metabolism of Pseudomonas putida KT2440 and Pseudomonas aeruginosa PAO1. Metab Eng 54, 35–53. https://doi.org/https://doi.org/10.1016/j.ymben.2019.01.008

Kukurugya, M.A., Mendonca, C.M., Solhtalab, M., Wilkes, R.A., Thannhauser, T.W., Aristilde, L., 2019. Multi-omics analysis unravels a segregated metabolic flux network that tunes co-utilization of sugar and aromatic carbons in Pseudomonas putida. Journal of Biological Chemistry 294, 8464–8479. https://doi.org/https://doi.org/10.1074/jbc.RA119.007885

Lewis, N.E., Hixson, K.K., Conrad, T.M., Lerman, J.A., Charusanti, P., Polpitiya, A.D., Adkins, J.N., Schramm, G., Purvine, S.O., Lopez-Ferrer, D., Weitz, K.K., Eils, R., König, R., Smith, R.D., Palsson, B.Ø., 2010. Omic data from evolved *E. coli* are consistent with computed optimal growth from genome‐scale models. Mol Syst Biol 6, 390. https://doi.org/https://doi.org/10.1038/msb.2010.47

Liu, D., Geiselman, G.M., Coradetti, S., Cheng, Y.-F., Kirby, J., Prahl, J.-P., Jacobson, O., Sundstrom, E.R., Tanjore, D., Skerker, J.M., Gladden, J., 2020. Exploiting nonionic surfactants to enhance fatty alcohol production in Rhodosporidium toruloides. Biotechnol Bioeng 117, 1418–1425. https://doi.org/https://doi.org/10.1002/bit.27285

Liu, D., Hwang, H.J., Otoupal, P.B., Geiselman, G.M., Kim, Joonhoon, Pomraning, K.R., Kim, Y.-M., Munoz, N., Nicora, C.D., Gao, Y., Burnum-Johnson, K.E., Jacobson, O., Coradetti, S., Kim, Jinho, Deng, S., Dai, Z., Prahl, J.-P., Tanjore, D., Lee, T.S., Magnuson, J.K., Gladden, J.M., 2023. Engineering Rhodosporidium toruloides for production of 3-hydroxypropionic acid from lignocellulosic hydrolysate. Metab Eng 78, 72–83. https://doi.org/https://doi.org/10.1016/j.ymben.2023.05.001

Liu, T., Mazmouz, R., Pearson, L.A., Neilan, B.A., 2019. Mutagenesis of the Microcystin Tailoring and Transport Proteins in a Heterologous Cyanotoxin Expression System. ACS Synth Biol 8, 1187–1194. https://doi.org/10.1021/acssynbio.9b00068

Llewellyn, C.A., Greig, C., Silkina, A., Kultschar, B., Hitchings, M.D., Farnham, G., 2020. Mycosporine-like amino acid and aromatic amino acid transcriptome response to UV and far-red light in the cyanobacterium Chlorogloeopsis fritschii PCC 6912. Sci Rep 10, 20638. https://doi.org/10.1038/s41598-020-77402-6

Miyamoto, K.T., Mamoru, K., Haruo, I., 2014. Discovery of Gene Cluster for Mycosporine-Like Amino Acid Biosynthesis from Actinomycetales Microorganisms and Production of a Novel

Mycosporine-Like Amino Acid by Heterologous Expression. Appl Environ Microbiol 80, 5028–5036. https://doi.org/10.1128/AEM.00727-14

Nikel, P.I., Chavarría, M., Fuhrer, T., Sauer, U., de Lorenzo, V., 2015. Pseudomonas putida KT2440 Strain Metabolizes Glucose through a Cycle Formed by Enzymes of the Entner-Doudoroff, Embden-Meyerhof-Parnas, and Pentose Phosphate Pathways * . Journal of Biological Chemistry 290, 25920–25932. https://doi.org/10.1074/jbc.M115.687749

Nikel, P.I., de Lorenzo, V., 2018. Pseudomonas putida as a functional chassis for industrial biocatalysis: From native biochemistry to trans-metabolism. Metab Eng 50, 142–155. https://doi.org/https://doi.org/10.1016/j.ymben.2018.05.005

Niu, W., Willett, H., Mueller, J., He, X., Kramer, L., Ma, B., Guo, J., 2020. Direct biosynthesis of adipic acid from lignin-derived aromatics using engineered Pseudomonas putida KT2440. Metab Eng 59, 151–161. https://doi.org/https://doi.org/10.1016/j.ymben.2020.02.006

Noel Jr., R.J., Reznikoff, W.S., 2000. Structural Studies of lacUV5-RNA Polymerase Interactions in Vitro: ETHYLATION INTERFERENCE AND MISSING NUCLEOSIDE ANALYSIS *. Journal of Biological Chemistry 275, 7708–7712. https://doi.org/10.1074/jbc.275.11.7708

Oliver, E.C.J., Donat, M.G., Burrows, M.T., Moore, P.J., Smale, D.A., Alexander, L. V, Benthuysen, J.A., Feng, M., Sen Gupta, A., Hobday, A.J., Holbrook, N.J., Perkins-Kirkpatrick, S.E., Scannell, H.A., Straub, S.C., Wernberg, T., 2018. Longer and more frequent marine heatwaves over the past century. Nat Commun 9, 1324. https://doi.org/10.1038/s41467-018-03732-9

Orfanoudaki, M., Hartmann, A., Alilou, M., Gelbrich, T., Planchenault, P., Derbré, S., Schinkovitz, A., Richomme, P., Hensel, A., Ganzera, M., 2020. Absolute Configuration of Mycosporine-Like Amino Acids, Their Wound Healing Properties and In Vitro Anti-Aging Effects. Mar Drugs 18. https://doi.org/10.3390/md18010035

Park, S.-H., Lee, K., Jang, J.W., Hahn, J.-S., 2019. Metabolic Engineering of Saccharomyces cerevisiae for Production of Shinorine, a Sunscreen Material, from Xylose. ACS Synth Biol 8, 346–357. https://doi.org/10.1021/acssynbio.8b00388

Perez-Riverol, Y., Bai, J., Bandla, C., García-Seisdedos, D., Hewapathirana, S., Kamatchinathan, S., Kundu, D.J., Prakash, A., Frericks-Zipper, A., Eisenacher, M., Walzer, M., Wang, S., Brazma, A., Vizcaíno, J.A., 2022. The PRIDE database resources in 2022: a hub for mass spectrometry-based proteomics evidences. Nucleic Acids Res 50, D543–D552. https://doi.org/10.1093/nar/gkab1038

Pope, M.A., Spence, E., Seralvo, V., Gacesa, R., Heidelberger, S., Weston, A.J., Dunlap, W.C., Shick, J.M., Long, P.F., 2015. O-Methyltransferase Is Shared between the Pentose Phosphate and Shikimate Pathways and Is Essential for Mycosporine-Like Amino Acid Biosynthesis in Anabaena variabilis ATCC 29413. ChemBioChem 16, 320–327. https://doi.org/https://doi.org/10.1002/cbic.201402516

Portwich, A., Garcia-Pichel, F., 2003. Biosynthetic pathway of mycosporines (mycosporine-like amino acids) in the cyanobacterium Chlorogloeopsis sp. strain PCC 6912. Phycologia 42, 384–392. https://doi.org/10.2216/i0031-8884-42-4-384.1

Qunjie, G., Ferran, G.-P., 2011. An ATP-Grasp Ligase Involved in the Last Biosynthetic Step of the Iminomycosporine Shinorine in Nostoc punctiforme ATCC 29133. J Bacteriol 193, 5923–5928. https://doi.org/10.1128/jb.05730-11

Rao, X., Li, D., Su, Z., Nomura, C.T., Chen, S., Wang, Q., 2024. A smart RBS library and its prediction model for robust and accurate fine-tuning of gene expression in Bacillus species. Metab Eng 81, 1–9. https://doi.org/https://doi.org/10.1016/j.ymben.2023.11.002

Roberto, D., Lucia, B., Cinzia, C., Donato, G., Elisabetta, D., Paola, A., Lucedio, G., Antonio, P., 2008. Sunscreens Cause Coral Bleaching by Promoting Viral Infections. Environ Health Perspect 116, 441–447. https://doi.org/10.1289/ehp.10966

Salis, H.M., 2011. Chapter two - The Ribosome Binding Site Calculator, in: Voigt, C. (Ed.), Methods in Enzymology. Academic Press, pp. 19–42. https://doi.org/https://doi.org/10.1016/B978-0-12-385120-8.00002-4

Schultz, J.C., Mishra, S., Gaither, E., Mejia, A., Dinh, H., Maranas, C., Zhao, H., 2022. Metabolic engineering of Rhodotorula toruloides IFO0880 improves C16 and C18 fatty alcohol production from synthetic media. Microb Cell Fact 21, 26. https://doi.org/10.1186/s12934-022-01750-3

Shetty, R.P., Endy, D., Knight, T.F., 2008. Engineering BioBrick vectors from BioBrick parts. J Biol Eng 2, 5. https://doi.org/10.1186/1754-1611-2-5

Silva, J.C., Gorenstein, M. V, Li, G.-Z., Vissers, J.P.C., Geromanos, S.J., 2006. Absolute Quantification of Proteins by LCMSE: A Virtue of Parallel ms Acquisition *S. Molecular & Cellular Proteomics 5, 144–156. https://doi.org/https://doi.org/10.1074/mcp.M500230-MCP200

Storch, M., Casini, A., Mackrow, B., Fleming, T., Trewhitt, H., Ellis, T., Baldwin, G.S., 2015. BASIC: A New Biopart Assembly Standard for Idempotent Cloning Provides Accurate, Single-Tier DNA Assembly for Synthetic Biology. ACS Synth. Biol. 4, 781.

Suh, S.-S., Hwang, J., Park, M., Seo, H.H., Kim, H.-S., Lee, J.H., Moh, S.H., Lee, T.-K., 2014. Anti-Inflammation Activities of Mycosporine-Like Amino Acids (MAAs) in Response to UV Radiation Suggest Potential Anti-Skin Aging Activity. Mar Drugs 12, 5174–5187. https://doi.org/10.3390/md12105174

Tao, L., Jackson, R.E., Cheng, Q., 2005. Directed evolution of copy number of a broad host range plasmid for metabolic engineering. Metab Eng 7, 10–17. https://doi.org/https://doi.org/10.1016/j.ymben.2004.05.006

Teresa, del C., L., R.J., J., R.-H.J., Tobias, F., Uwe, S., Estrella, D., 2007. Convergent Peripheral Pathways Catalyze Initial Glucose Catabolism in Pseudomonas putida: Genomic and Flux Analysis. J Bacteriol 189, 5142–5152. https://doi.org/10.1128/JB.00203-07

Tian, T., Kang, J.W., Kang, A., Lee, T.S., 2019. Redirecting Metabolic Flux via Combinatorial Multiplex CRISPRi-Mediated Repression for Isopentenol Production in Escherichia coli. ACS Synth Biol 8, 391–402. https://doi.org/10.1021/acssynbio.8b00429

Tiso, T., Sabelhaus, P., Behrens, B., Wittgens, A., Rosenau, F., Hayen, H., Blank, L.M., 2016. Creating metabolic demand as an engineering strategy in Pseudomonas putida – Rhamnolipid synthesis as an example. Metab Eng Commun 3, 234–244. https://doi.org/https://doi.org/10.1016/j.meteno.2016.08.002

Torres, P., Santos, J.P., Chow, F., Pena Ferreira, M.J., dos Santos, D.Y.A.C., 2018. Comparative analysis of in vitro antioxidant capacities of mycosporine-like amino acids (MAAs). Algal Res 34, 57–67. https://doi.org/https://doi.org/10.1016/j.algal.2018.07.007

Tsuge, Y., Kawaguchi, H., Yamamoto, S., Nishigami, Y., Sota, M., Ogino, C., Kondo, A., 2018. Metabolic engineering of Corynebacterium glutamicum for production of sunscreen shinorine. Biosci., Biotechnol., Biochem. 82, 1252.

Wada, N., Sakamoto, T., Matsugo, S., 2015. Mycosporine-Like Amino Acids and Their Derivatives as Natural Antioxidants. Antioxidants 4, 603–646. https://doi.org/10.3390/antiox4030603

Wang, J., Jiang, T., Milligan, S., Zhang, J., Li, C., Yan, Y., 2022. Improving isoprenol production via systematic CRISPRi screening in engineered Escherichia coli. Green Chemistry 24, 6955–6964. https://doi.org/10.1039/D2GC02255A

Wang, X., Baidoo, E.E.K., Kakumanu, R., Xie, S., Mukhopadhyay, A., Lee, T.S., 2022. Engineering isoprenoids production in metabolically versatile microbial host Pseudomonas putida. Biotechnology for Biofuels and Bioproducts 15, 137. https://doi.org/10.1186/s13068-022-02235-6

Wang, Yan, Horlamus, F., Henkel, M., Kovacic, F., Schläfle, S., Hausmann, R., Wittgens, A., Rosenau, F., 2019. Growth of engineered Pseudomonas putida KT2440 on glucose, xylose, and arabinose: Hemicellulose hydrolysates and their major sugars as sustainable carbon sources. GCB Bioenergy 11, 249–259. https://doi.org/https://doi.org/10.1111/gcbb.12590

Wang, Ying, Ling, C., Chen, Y., Jiang, X., Chen, G.-Q., 2019. Microbial engineering for easy downstream processing. Biotechnol Adv 37, 107365. https://doi.org/https://doi.org/10.1016/j.biotechadv.2019.03.004

Wehrs, M., Gladden, J.M., Liu, Y., Platz, L., Prahl, J.-P., Moon, J., Papa, G., Sundstrom, E., Geiselman, G.M., Tanjore, D., Keasling, J.D., Pray, T.R., Simmons, B.A., Mukhopadhyay, A., 2019. Sustainable bioproduction of the blue pigment indigoidine: Expanding the range of heterologous products in R. toruloides to include non-ribosomal peptides. Green Chemistry 21, 3394–3406. https://doi.org/10.1039/C9GC00920E

Wen, Z., Zhang, S., Odoh, C.K., Jin, M., Zhao, Z.K., 2020. Rhodosporidium toruloides - A potential red yeast chassis for lipids and beyond. FEMS Yeast Res 20, foaa038. https://doi.org/10.1093/femsyr/foaa038

Wohlers, K., Wirtz, A., Reiter, A., Oldiges, M., Baumgart, M., Bott, M., 2021. Metabolic engineering of Pseudomonas putida for production of the natural sweetener 5-ketofructose from fructose or sucrose by periplasmic oxidation with a heterologous fructose dehydrogenase. Microb Biotechnol 14, 2592–2604. https://doi.org/https://doi.org/10.1111/1751-7915.13913

Yang, G., Cozad, M.A., Holland, D.A., Zhang, Y., Luesch, H., Ding, Y., 2018. Photosynthetic Production of Sunscreen Shinorine Using an Engineered Cyanobacterium. ACS Synth Biol 7, 664–671. https://doi.org/10.1021/acssynbio.7b00397

Yunus, I.S., Anfelt, J., Sporre, E., Miao, R., Hudson, E.P., Jones, P.R., 2022. Synthetic metabolic pathways for conversion of CO2 into secreted short-to medium-chain hydrocarbons using cyanobacteria. Metab Eng 72, 14–23. https://doi.org/https://doi.org/10.1016/j.ymben.2022.01.017

Yunus, I.S., Jones, P.R., 2018. Photosynthesis-dependent biosynthesis of medium chain-length fatty acids and alcohols. Metab Eng 49. https://doi.org/10.1016/j.ymben.2018.07.015

Yunus, I.S., Palma, A., Trudeau, D.L., Tawfik, D.S., Jones, P.R., 2020. Methanol-free biosynthesis of fatty acid methyl ester (FAME) in Synechocystis sp. PCC 6803. Metab Eng 57, 217–227. https://doi.org/https://doi.org/10.1016/j.ymben.2019.12.001

Zhao, D., Zhu, X., Zhou, H., Sun, N., Wang, T., Bi, C., Zhang, X., 2021. CRISPR-based metabolic pathway engineering. Metab Eng 63, 148–159. https://doi.org/https://doi.org/10.1016/j.ymben.2020.10.004